Volume 12
Issue 2
December 2023

ISSN - 1857 - 839X

SJCE
SCIENTIFIC JOURNAL OF CIVIL ENGINEERING

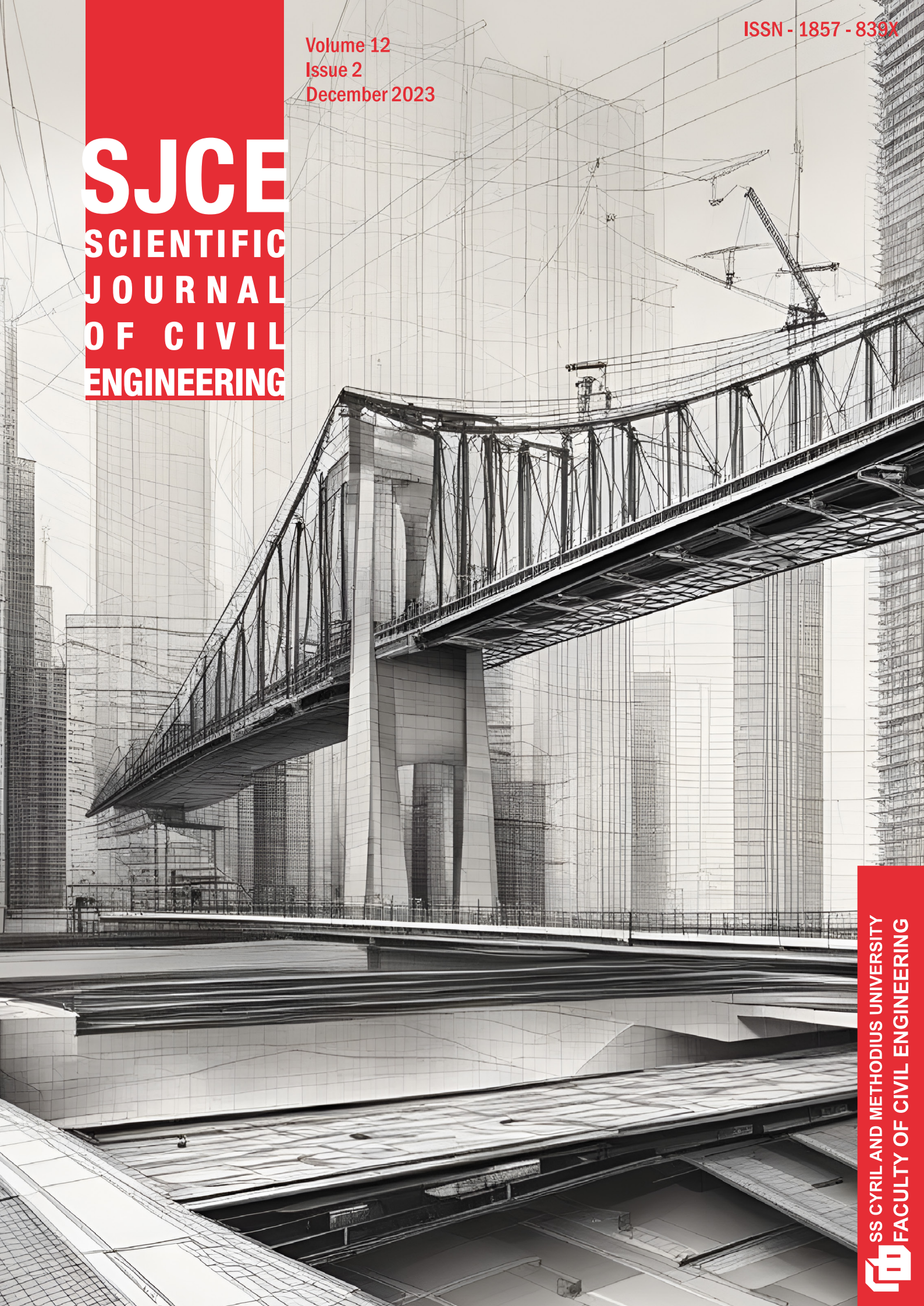

SS CYRIL AND METHODIUS UNIVERSITY
FACULTY OF CIVIL ENGINEERING

EDITORIAL - Preface to Volume 12 Issue 2 of the Scientific Journal of Civil Engineering (SJCE)

Vladimir Vitanov EDITOR - IN - CHIEF

Dear Readers,

The **S**cientific **J**ournal of **C**ivil **E**ngineering (SJCE) is an international, peer-reviewed, open-access journal, initiated in December 2012, and distributed bi-annually. As of December 2021, SJCE has launched its dedicated website and transitioned to a fully digital platform for submission, review, and publication processes. For further details regarding the online edition of the Journal, kindly visit www.sjce.gf.ukim.edu.mk.

At SJCE, we are dedicated to publishing and disseminating high-quality, innovative scientific research across the broad field of engineering sciences. Our journal aims to advance technical knowledge and promote cutting-edge engineering solutions in civil engineering, geotechnics, surveying and geo-spatial engineering, environmental protection, construction management, and related areas.

As the Editor-in-Chief of the Scientific Journal of Civil Engineering, it gives me great pleasure to present to you the second issue of Volume 12, an open-subject issue. Seven scientific research papers that have successfully undergone the established review process of this journal are presented in this issue.

The first paper reviews the seismic risk assessment of Strumica, North Macedonia, focusing on the vulnerability of buildings, particularly the PHI “General Hospital Strumica,” and emphasizes the importance of socio-economic factors in understanding and mitigating earthquake impacts. The second paper investigates soil-structure interaction using a small-scale steel frame model on a shaking table, comparing fixed base and sand bed foundations under dry and saturated conditions to study the impact of soil stiffness on structural behavior during dynamic excitation. The study presented in the third paper highlights the significant role of green spaces in reducing urban heat island effects and mitigating thermal stress in Skopje, emphasizing the need for urban planning strategies that integrate green infrastructure to combat climate change and promote public health. In the fourth paper, a review of research in the area of new method for addition of bacteria in concrete is given. The addition of bacteria to concrete has shown promise in self-healing cracks by precipitating calcium carbonate, but while effective in healing cracks up to 0.97 mm, it introduces complications in the preparation process and requires further study on encapsulation materials, incubation conditions, and sustainability. The fifth paper evaluates the behavior of steel moment frames under dynamic loads, focusing on the rationality of the interstory drift sensitivity coefficient θ through non-linear static analysis, and compares the results with Eurocode 8 criteria. The sixth paper explores the use of innovative materials, particularly CFRP, for repairing and strengthening RC buildings in seismic regions, focusing on cases where the built-in concrete did not meet design specifications. The final paper explores the use of straw in cement composites to enhance thermal insulation and sustainability in construction, looking for the sutable percentage of straw content that optimizes the thermal properties while maintaining good mechanical strength.

The insights provided in this issue have the potential to significantly advance our understanding of the various issues in civil engineering, paving the way for further developments. I extend my deepest gratitude to the authors, reviewers, and editorial team for their dedication and hard work in bringing this issue to fruition.

Sincerely,

Vladimir Vitanov, Editor-in-Chief

December 2023

SJCE
SCIENTIFIC JOURNAL OF CIVIL ENGINEERING

Impressum

FOUNDER AND PUBLISHER

Faculty of Civil Engineering
Partizanski odredi 24, 1000
Skopje, N. Macedonia

PRINT

This Journal is printed in Mar-saz DOOEL Skopje

EDITORIAL OFFICE

Faculty of Civil Engineering
Partizanski odredi 24, 1000
Skopje, N. Macedonia
tel. +389 2 3116 066
fax. +389 2 3118 834
prodekan.nauka@gf.ukim.edu.mk

EDITOR IN CHIEF

Prof. PhD **Vladimir Vitanov**
Ss. Cyril and Methodius University in Skopje
Faculty of Civil Engineering
Partizanski odredi 24, 1000
Skopje, N. Macedonia
v.vitanov@gf.ukim.edu.mk

ISSN: 1857-839X

SJCE
SCIENTIFIC JOURNAL OF CIVIL ENGINEERING

Impressum

ORDERING INFO

SJCE is published bi-annually.
All articles published in the journal have been reviewed.

Edition: 100 copies

SUBSCRIPTIONS

Price of a single copy:
for Macedonia (500 den);
for abroad (10 EUR + shipping cost).

BANKING DETAILS (NORTH MACEDONIA)

Narodna banka na RNM
Account number:
160010421978815
Prihodno konto 723219,
Programa 41

BANKING DETAILS (INTERNATIONAL)

Correspond bank details:
Deutsche Bundesbank Zentrale
Address: Wilhelm Epstein Strasse 14 Frankfurt am Main, Germany
SWIFT BIC: MARK DE FF
Bank details:
National Bank of the RNM
Address: Kompleks banki bb 1000 Skopje, North Macedonia
SWIFT BIC: NBRM MK 2X
IBAN: MK 07 1007 0100 0036 254
Name: Gradezen fakultet Skopje

SELECT A PROFESSION

CREATIVE	SOPHISTICATED	RECOGNIZED	RESPONSIBLE
ENDURING	UP-TO-DATE	WORLWIDE	IMPORTANT

WWW.GF.UKIM.EDU.MK

OUR FACULTY CAN GIVE YOU

IMPULSE !	SCHOLARSHIPS FOR THE BEST	ASSURANCE !	COORPERATION WITH INDUSTRY AND INTERNATIONAL UNIVERSITIES
SIMPLE ENROLLMENT	MOTIVATION !	100% EMPLOYMENT AND INTERNATIONALLY RECOGNIZED DIPLOMA	SUPPORT !

WWW.GF.UKIM.EDU.MK

SJCE
SCIENTIFIC JOURNAL OF CIVIL ENGINEERING

CONTENTS

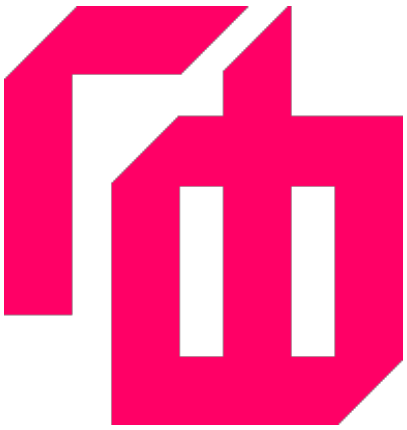

СЕКОГАШ БИДИ ИН

WWW.GF.UKIM.EDU.MK

Nadica Angova Kolevska
MSc
Ss. Cyril and Methodius University in Skopje
Institute of Earthquake Engineering and Engineering Seismology
N. Macedonia
nadica_angova@hotmail.com

Marija Vitanova
PhD, Associate Professor
Ss. Cyril and Methodius University in Skopje
Institute of Earthquake Engineering and Engineering Seismology
N. Macedonia

A CONTRIBUTION IN SEISMIC RISK ASSESSMENT IN STRUMICA - A CASE STUDY FOR THE PHI "GENERAL HOSPITAL" STRUMICA

The increase in the number of inhabitants in the cities as a result of increasingly pronounced rural-urban migration and their concentration in densely populated areas in modern societies, nowadays, has led to an increase in the need to be alert to the impact of catastrophic natural events, earthquakes in particular. The devastating earthquakes that have hit the territory of Europe in the last 20 years have led to an increase in interest and expansion of knowledge about the seismic vulnerability of buildings in Europe. In this study, a review of the seismic risk assessment in the city of Strumica (the largest town in the Southeastern planning region and the tenth largest city in North Macedonia [1]), regarding hazard, exposure, and vulnerability of buildings, with a focus on PHI "General Hospital Strumica" is presented. The proposed methodology for seismic risk assessment consists of defining hazard assessment method to estimate the maximum level of ground motion that could occur at the site, collecting and harmonizing available data for the existing build construction fund in the city and developing tools and methods, based on which an exposure model of the city is created and fragility models are applied to further estimate the expected damages to the buildings located in the city. The results will allow a better understanding of the level of vulnerability of the existing buildings in the analyzed region, emphasizing the importance of socio-economic variables. The collected database could be updated and further developed.

Keywords: seismic vulnerability, hazard, exposure, damages

1. INTRODUCTION

Looking back chronologically, the number of disasters worldwide in recent years has increased rapidly, causing more damage and deaths. Earthquakes, floods, landslides, and other natural disasters cause irreparable damage, threatening people's lives, crops

material resources, and the built environment [2] [3]. With the rapid growth of earthquakes as natural disasters, their consequences are becoming more serious, including significant damage to buildings, existing infrastructure, and the societies themselves. To reduce the impact of earthquakes on engineering structures, a logical approach and assessment of the effects of earthquakes on buildings - and more importantly, on people - is required [4], [5]. To this end, various seismic risk assessment methods have been developed, by which the risk is measured. The first step in the seismic risk assessment process is to estimate the earthquake hazard in a given geographic area/region. For this study, two extreme earthquake scenarios from past earthquakes that affected the city were selected, with parameters of which hazard model is created: the Pehchevo-Kresna earthquake (1904) with a maximum rupture strength of 7.8 MCS and the Valandovo-Dojran earthquake (1931) with a maximum rupture strength of 6.7 MCS [6]. Then, based on the available data, building taxonomies for the building stock were created, using the taxonomy scheme of the Global Earthquake Model (GEM), which allows buildings to be classified according to several structural attributes, i.e., main construction material, number of stories, age of construction and seismic design level [7], and exposure model of the city was developed. The fragility assessment method was presented by choosing existing fragility curves for the building stock in the city which is expected to lead to creating damage maps of the city's stocks and analyzing uncertainties in earthquake risk assessment analysis. The applied methodology can be of particular interest to the national authorities as they implement new policies and strategies in the planning process.

2. SEISMIC HAZARD ASSESSMENT OF STRUMICA CITY

In this study, deterministic seismic hazard assessment (DSHA) is used as a method for estimating the maximum level of ground motion that could occur at a particular site [8]. To validate the seismic risk methodology for the city of Strumica and the PHI "General Hospital" two seismic scenarios are used, which represent the two most destructive past earthquakes that have affected the study area: the Pehcevo-Kresna (1904) Mw.7.8 earthquake and the Valandovo-Dojran (1931) Mw.6.7 earthquake [6]. The two events were simulated in OpenQuake Engine [9] as earthquake rupture scenarios. For both earthquakes, we used the ESHM20-Active faults model developed as an update of the European Database of Seismogenic Faults 2013 [10]. Strong ground motion modeling was performed using the ground-motion prediction equation (GMPE) by the Abrahamson EtAl2015Sinter model [11]. To account for local site conditions of Strumica City, the applied GMPE [11] uses as site parameters the Vs.30. i.e. the average shear wave velocity of the upper 30m of the soil profile, calculated from the total time needed for a shear wave to travel this 30 m. This parameter is contained in Site conditions North Macedonia that we use in our study as a required parameter for the earthquake rupture scenarios [12]. Figures 1 and 2 illustrate the spatial distribution of peak ground acceleration PGA (g) for the city of Strumica obtained from the Pehcevo-Kresna (1904) (Figure 1) and Valandovo - Dojran (1931) scenario (Figure 2) made with OpenQuake Engine, using the fault rupture model by ESHM20 [10], the Abrahamson EtAl2015Sinter GMPE [11] and the Vs.30 site parameter contained in Site Conditions North Macedonia [13]. It is observed that the PGA values estimated with the

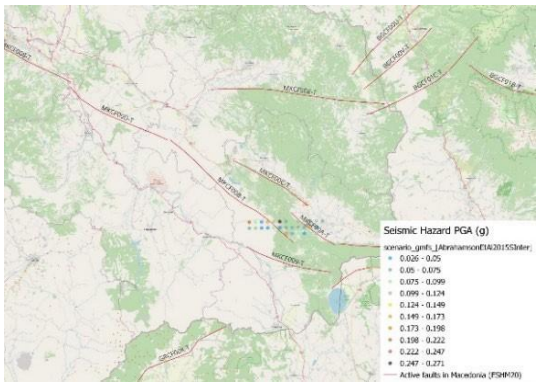

Figure 1. Pehchevo-Kresna Mw.8.7:PGA values obtained from scenario analysis with OpenQuake using the fault rupture model by ESHM20 [10]

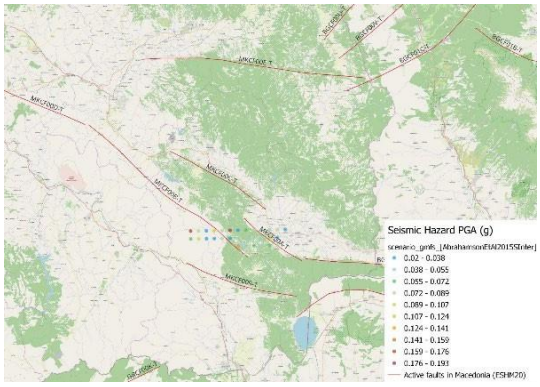

Figure 2. Valandovo-Dojran Mw.6.7.PGA values obtained from scenario analyses with OpenQuake using the fault rupture model by ESHM20 [10]

OpenQuake for the scenario Pehcevo-Kresna (1904) range between 0.198 g and 0.222 g and for the Valandovo - Dojran scenario range between 0.141 g and 0.159 g for the city of Strumica.

The range of ground shaking intensity according to the selected GMPE [11] shows that close to the fault we have a much higher intensity while the intensity decreases with increasing distance from the fault. What is important to mention is that each GMPE gives a very different prediction of the ground shaking because of the parameters contained [14].

3. EXPOSURE MODEL

3.1. A REVIEW OF EXISTING BUILDING TAXONOMIES IN THE CITY

A widely accepted qualitative definition of earthquake exposure is the tendency of a category of elements to be at risk of being damaged by potential earthquakes [15]. For large-scale assessments, to unequivocally demonstrate the assignment of a vulnerability model to an individual building, specific risk-oriented taxonomies are commonly applied. One of the most commonly used and also applied in this study is the taxonomy developed by GEM (Global Earthquake Model) [7], where single structures are described in detail from a functional and structural point of view. Using the building taxonomy scheme developed by GEM (GEM building taxonomy scheme) [7] the existing building stock in Strumica which contains a total of 4367 buildings is classified according to four (4) attributes: main constructional material, story height above the ground, year of construction (seismic code), or ductility of the building (Figure 3). The applied taxonomy used for creating an exposure model of the city is based on expert judgment, a combination of data collected by authorities, and field data collection.

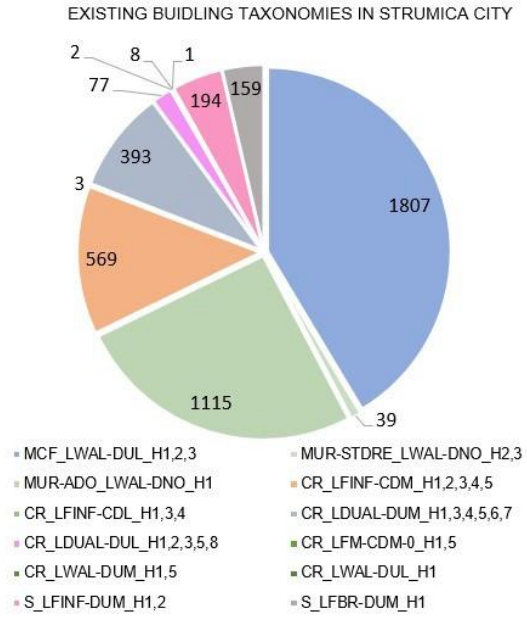

Figure 3. Displaying data from the Strumica database

Figure 4 Existing Building Taxonomies in Strumica Using QGIS classified by material and load-resisting structure

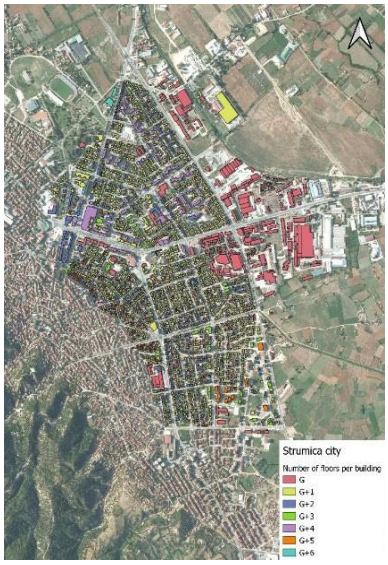

Figure 5. Existing Building Taxonomies in Strumica Using QGIS classified by the number of floors above ground

The obtained results for the building stock at a city level (4367 buildings) presented in Figure 3,4,5 show that in terms of construction material, masonry buildings are represented with a total number of 2961 buildings or 67.7%. Reinforced concrete buildings at the city level

are represented by a total number of 1053 buildings or 34.4%. Steel constructions at the city level are represented by a total number of 353 buildings or 8.08%. Regarding the height of the buildings, the largest number of buildings at the city level: 1873 buildings are ground-floor buildings (G) (Figure 5). Regarding the ductility of the buildings, most of the analyzed buildings at the city level: 2181 buildings show low ductility (built in the period 1964-1981). Regarding the period of construction of the buildings and the implementation of the codes for seismic design, the largest number of buildings, or a total of 2184 buildings, were built in the period 1964-1981 (moderate code level) following the regulations for seismic design resistant buildings, adopted in 1964 (JUS39/64) [16].

3.2. BUILDING TYPOLOGIES FOR THE PHI "GENERAL HOSPITAL" STRUMICA

The first beginnings of the Hospital Campus are dated to 1970 [17]. To meet the increased demands of the growing city for healthcare facilities, from 1970 until today, 7 separate buildings as part of the pavilion-type hospital complex, were built: Infectious Disease Building (1), Administrative building (2), Dermatologic clinic (3), Main building (4), Admission - discharge (5), Physical therapy and rehabilitation with laboratory with pathology and Radiology (6), New Hospital wing (7). The taxonomy classification shown in Figure 6,7 was created online through GEM (Pavia) v.2.0 taxonomy of high-rise buildings according to the GEM building taxonomy [7]. Two important parameters such as structural cost for each building individually, a value obtained by using an Official form for determining the value of the building per m^2 prescribed in the Methodology for determining the value of the building [18], and an exact number of users/patients in each facility within the hospital complex at different times of the day, day/night/transit, obtained through field data collection and interviews with hospital campus employees were also used in creating a relevant exposure model. A general survey of the facilities at PHI "General Hospital" Strumica (Figure 6) shows that the total net building area belongs to RC buildings. In terms of building height (Figure 7), the hospital campus is dominated by G+1 buildings (1,2,3), but there are also ground-floor buildings (G) (5,6), and 5-story- buildings (4,7). The filed data collection process has shown that all the facilities in the PHI "General Hospital" Strumica (except the New Wing (7) which was built in 2021 and is still not in use) were built in the period 1964-1981, taking into consideration the first Seismic Design Code, the "Temporary Regulations for Construction in Seismic Regions", Official Gazette of SFRY No. 39/64, enforced in 1964 [16].

Figure 6. Existing Building Taxonomies in PHI "General Hospital" Strumca using QGIS classified by material and load-resisting structure

Figure 7. Existing Building Taxonomies in PHI "General Hospital" Strumca using QGIS classified by the number of floors above ground

4. SEISMIC FRAGILITY CURVES FOR THE EXISTING BUILDING STOCK IN THE HOSPITAL COMPLEX

Assessing seismic fragility is an important step in determining the likelihood of seismic hazards [19]. Therefore, the methodology adopted in this study was based on the fragility curves derived from the database of existing fragility curves for European building classes [20] (classified using GEM Building Taxonomy [7]) developed as part of the SERA project, using publicly available resources and information for 44 European countries, covering the territory of RNM. It is based on ground motion records from both active subduction and shallow tectonic situations [20] for the covering areas. For the Hospital complex, in particular, it was

decided to apply the following fragility curves: first, the fragility curve developed for building taxonomy CR/LFINF by Kostov et al.[21] which contains 1-6 story CR buildings with infilled frames constructed after 1945, with a defined geographical origin Republic of Bulgaria (Figure 8) and the fragility curve developed for building taxonomy CR/LDUAL by Kappos et al. [22] with infilled dual systems with a defined geographical origin Republic of Greece (Figure 9). Both of them include building classes which seem to correspond well with the building stock of Strumica city. In the first curve, four damage states were considered ranging from light to complete damage, compared to the second one where 5 damage states were considered: from no damage (Grade 1) to complete damage (Grade 5). According to the building class properties, one intensity measure (PGA) has been considered. Both curves adopted in this study, adopt the same damage states and fragility curves are derived in terms of peak ground acceleration.

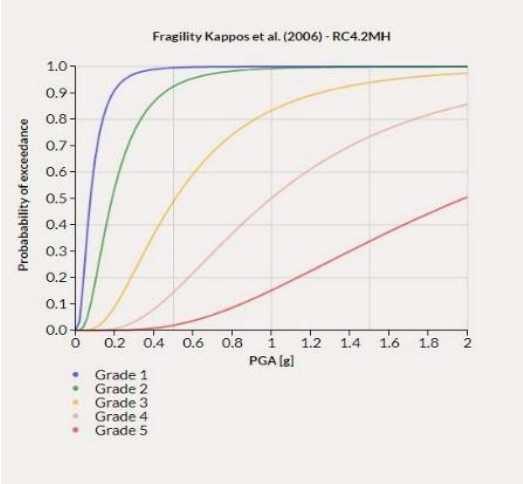

Figure 8. Existing fragility curve for structure class- building taxonomy CR_LFINF [21]

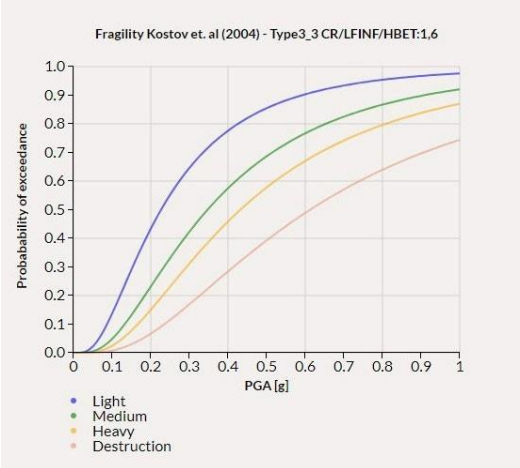

Figure 9. Existing fragility curve for structure class- building taxonomy CR_LDUAL [22]

5. CONCLUSION

Advanced disaster risk management recommends using risk-based data to develop strategies and measures based on scientific evidence [19]. Effective risk outcomes inform capacity building and management during the response and preparedness phases. The methodology presented in this study ensures the creation of a framework for further development of seismic risk analysis in the form of damage and loss maps for the existing building stock in the city. Based on seismic records from two seismic scenarios which represent the two most destructive past earthquakes that have affected the study area: the Pehcevo-Kresna (1904) Mw.7.8 earthquake and the Valandovo-Dojran (1931) Mw.6.7 earthquake [6], simulated in OpenQuake Engine software [14], as earthquake rupture scenarios, and with the use of the ESHM20-Active faults model as a layout, strong ground motion modeling was performed using the ground-motion prediction equation (GMPE) by the Abrahamson EtAl2015Sinter model [11] and the spatial distribution of peak ground acceleration PGA (g) for Strumica obtained from both scenarios was presented (Figure 1,2). After validating the seismic hazard methodology, the second step was to collect the building classes of interest. The output of the survey allowed us to identify the initial building classes in the Strumica database, and their classification according to the building taxonomy scheme developed by GEM [7] to be made. Collected data such as main building material, lateral load resisting system, period of construction and number of stories (height), structural cost, and occupants per building were used in the creation of the exposure model of the city, and through a process of vectorization and attribution of the real estate (objects) performed in two software platforms (CAD and GIS), analysis of the stock were made. The list of data can be further expanded to meet the requirements of the growing city in the future. In the final step, fragility models from the European Seismic Risk Model (ESRM20) [20] database, which comprises the building classes in the chosen area, was assessed and applied. The hazard, exposure, and fragility models, presented in this paper, can be applied to estimate the expected damages to the buildings located in Strumica city, for the Pehcevo-Kresna (1904) and Valandovo-Dojran (1931) earthquakes, respectively. The adoption and use of the described methodology can greatly contribute to increasing the resilience of cities.

Acknowledgments

The material presented in the paper is based on the work supported by the Agency of Cadastre of North Macedonia, Public enterprise for managing residential and business space in the Republic of North Macedonia, Municipality of Strumica, and the Department of Urbanism which greatly helped the process of gathering reliable data on the existing building stock in the city during the production of the primary version of this study.

6. REFERENCES

[1] "https://adsdp.com.mk/," [Online].

[2] „https://mk.wikipedia.org/wiki/%D0%A1%D1%82%D1%80%D1%83%D0%BC%D0%B8%D1%86%D0%B0," [Online].

[3] Abrahamson, N., Gregor, N., Addo, K., (2016), "BC Hydro Ground Motion Prediction Equations for Subduction Earthquakes," Sage Journals, vol. 32, no. 1, pp. 36.

[4] Alizadeh, M., Alizadeh, E., Asadollahpour Kotenaee, S., Shahabi, H., Beiranvand Pour, A., Panahi, M., Bin Ahmad, B., Saro,L.,(2018), "Social Vulnerability Assessment Using Artificial Neural Network (ANN) Model for Earthquake Hazard in Tabriz City, Iran," Sustainability, vol. 10, pp. 23.

[5] Azizi, A., Yaghoobi, M., Kamel, R., (2023) "Earthquake risk assessment using OpenQuake and GIS: A case study of Cyprus," GeoInformatica, pp. 30.

[6] Basili, R., Danciu, L., Carafa, M., Kastelic, V., Maesano, F., Vallone, R., Gracia, E., Sesetyan, K., Atanackov, J., Sket- Motnikar, B., Zupančič, P., Vanneste, K., Vilanova, S., (2020), "Insights on the European Fault-Source Model (EFSM20) as input to the 2020 update of the European Seismic Hazard Model (ESHM20)," EGU General Assembly.

[7] CEN. (2008), "Eurocode 8: Design of structures for earthquake resistance - Part 1: General rules, seismic actions and rules for buildings, European Standard EN 1998-1:2004.," European Committee for Standardisation, Brussels.

[8] Crowley, H., Dabbeek, J., Despotaki, V., Rodrigues, D., Martins, L., Silva, V., Romão, X., Pereira, N., Weatherill, G., Danciu, L., (2021), "European Seismic Risk Model (ESRM20). EFEHR Technical Report," 2021-02 V1.0.0.

[9] Danciu, L., Nandan, L., Reyes, C., Basili, R., Weatherill, G., Beauval, C., Rovida, A., Vilanova, K., Bard, P., Cotton, F., Wiemer S., Giardini, D (2021), "The 2020 update of the European Seismic Hazard Model," EFEHR, Zurich.

[10] GEM. (2022) "The OpenQuake User Manual for Engine version 3.15.0," Global Earthquake Model (GEM), Pavia.

[11] Kappos, A., Panagopoulos, G., Panagiotopoulos, C., et al (2006), "A hybrid method for the vulnerability assessment of R/C and URM buildings,"Bull Earthquake Eng, vol. 4, pp. 391–413.

[12] Kocubovski,M.,Spasenovska, M., (2012), "Podgotvenost za odgovor na zdravstveniot sistem vo opshtina Strumica pri masovni nesreki," Skopje.

[13] Kostov, M.,Vaseva, E.,Kaneva, A., Koleva, N., Varbanov, G., Stefanov, D., Darvarova, E., Solakov, D., Simeonova, S.,Cristoskov,L., (2004), "Application to Sofia, Report RISK-UE WP13," RISK-UE WP13.

[14] Pavic, G., Hadzima-Nyarko, M, Bulajic, B. (2020), "A Contribution to a UHS-Based Seismic Risk Assessment in Croatia—A Case Study for the City of Osijek," Sustainability, vol. 12(5), no. 1796.

[15] Salic Makreska, R., Milutinovic, Z., Garevski, M. (2019), "Results Achieved and Improvements Needed in the Field of Seismic Hazard Assessment of Republic of Macedonia," in 15th World Conference on Earthquake Engineering, Lisbon.

[16] Nikoo, M., Ramezani, F., Hadzima- Nyarko, M., Nyarko, E., Nikoo, M., (2016), "Flood-routing modeling with neural network optimized by social-based algorithm," Natural Hazards 82 (1), vol.82, pp. 1-24.

[17] Işık, E. (2016), "Consistency of the rapid assessment method for reinforced concrete buildings," Earthq. Struct., vol. 11, pp. 873–885.

[18] Hadzima-Nyarko, M., Pavić, G., Lešić, M., "Seismic vulnerability of old confined masonry buildings in Osijek, Croatia," Earthq. Struct., vol. 11, pp. 629–648.

[19] Eleftheria, P., Karakostas, V., Tranos, M.D., Ranguelov, B., (2007) "Static stress changes associated with normal faulting earthquakes in South Balkan area," International Journal of Earth Sciences, vol. 96, pp. 911–924.

[20] Brzev, S., Scawthorn, C., Charleson, A., Allen, L.,Greene, M., Jaiswal, K., Silva, V., (2013), "GEM Building Taxonomy Version 2.0, GEM Technical Report 2013- 02 V1.0.0," GEM Foundation, Pavia, Italy.

[21] Huang, D., Wang, J., Brant, L., Chang, S.,(2012), "Deterministic Seismic Hazard Analysis Considering Non-controlling Seismic Sources and Time Factors," in International Conference on Scalable Uncertainty Management, Marburg.

[22] Pagani, M., Monelli, D., Weatherill, G., Danciu, L., Crowley, H., Silva, V., Henshaw, P., Butler, L., Nastasi, M., Panzeri, L., Simionato, M., Vigano, D., (2014) "OpenQuake Engine: An open hazard (and risk) software for the Global Earthquake Model," Seismological Research Letters, vol. 85, no.3.

Adriana Brandis
Postdoctoral researcher
Faculty of Civil Engineering and Architecture Osijek
Croatia
acerovecki@gfos.hr

Nina Cheh
PhD, Assistant professor
Faculty of Civil Engineering Rijeka
Croatia

Vedran Jagodnik
PhD, Professor
Faculty of Civil Engineering Rijeka
Croatia

Ivan Kraus
PhD, Professor
Faculty of Civil Engineering and Architecture Osijek
Croatia

Denis Brandis
MSc
Brand-ing d.o.o.
Croatia

DYNAMIC BEHAVIOUR OF SOIL-STEEL FRAME SYSTEMS: A SHAKING TABLE EXPERIMENT

This paper presents an experimental investigation of soil-structure interaction. The study tests a small-scale steel frame model using shaking table. The model features two columns, connected by a foundation beam and a girder at the top with the superstructure's mass. The testing encompassed two distinct configurations: first where the model was fixed to the shaking platform and second where the model was placed on a sand bed. Throughout the experiments, displacements were meticulously recorded over time, by a system for optical measurement. A local Drava sand was chosen for the experiment. Notably, the experiments were conducted under both dry and saturated conditions. Analyzing the results one can conclude that fixed base models have different behaviour compared to models founded on soil. Stiffness of the soil has a big impact on the behaviour of the soil-structure system where stiffer foundation soil results with behaviour closer to fixed base case while the flexible soil changes behaviour of the models considering the displacements which are the result of dynamic excitation.

Keywords: experiment, soil-structure interaction, shaking table, small-scale model, optical measurement

1. INTRODUCTION

Soil-structure interaction remains attractive research topic for numerous researchers [1-3]. Many of researchers base their studies on data acquired through either field-based or laboratory-based experimental measurements. After a brief literature review, it becomes evident that three types of experiments are most frequently employed in the examination of soil-structure interaction: (i) centrifuge tests, (ii) shaking table tests, and (iii) in-situ tests.

Centrifuge tests are particularly informative in the realm of geotechnical research, although their smaller scale looks for a comparison with experiments conducted in a larger scale. Larger-scale models facilitate the incorporation of larger measuring instruments and more closely emulate the behavior of real-world systems.

Although large-scale experiments are encouraged, due to their high costs and laboratory limitations, they are not always possible. Considering all limitations, original experimental research of soil-structure interaction is planned and carried out by the authors. The main goal of the research was to investigate the impact of foundation soil flexibility on the seismic behaviour of the structures with shallow foundations through original experimental research on small-scale models and parametric analysis.

Furthermore, in order to investigate soil structure interaction, experimental research studied by other authors are briefly presented Prevost and Scanlan's study in 1983 [4] delved into the dynamic effects of soil-structure interaction. Their research involved subjecting individual piles, groups of piles, and a shallow circular foundation to testing in a geotechnical centrifuge. The Knappett et al [5] studied the mechanisms underlying the failure of foundation load-bearing capacity under seismic loads where foundation strips were tested using a shaking platform. Research from 2010 by Anastasopoulos [1] conducted experiments with an inverted pendulum clamped to a square base foot, tested in a shear box on a shaking platform. Pender et al [6] explored the behavior of tilting and rocking of shallow foundations subjected to cycling loading in situ. Abate and Massimino [7] focused on the effects of dynamic interaction among soil, foundation, and structure. Their experimental setup involved testing of a steel 3D frame on a foundation plate using shaking platform, unveiling the dynamic behaviors and responses within such systems. Further research by Pender et al[8] studied soil-structure interaction through centrifuge experiment using simple two-dimensional models with square foundations in geotechnical centrifuges. Dynamic 3D tests were conducted by Hirave and Kalyanshetti [9] testing a foundation plate on a shaking platform. Finally, in 2019, Kumar and Mishra [3] explored the influence of structure characteristics on soil-structure interaction. Their research involved employing 3D models of structure on foundation slabs, single foundations, and foundation strips on a shaking platform, offering valuable insights into how diverse structural attributes, such as foundation slabs, single foundations or foundation strips, impact the interaction with the underlying soil.

Collectively, all of these studies contribute to a comprehensive understanding of soil-structure interaction and were used as a guideline in designing of experimental research conducted by the authors.

2. EXPERIMENTAL SETUP

Dynamic effects of soil-structure interaction were observed on a scaled model Comparable experimental investigations of the same nature and scale can also be found in [5, 10, 11]. As part of the project, dynamic tests were carried out on a scaled frame model with varying foundation conditions. Initially, the model was fixed at the foundation level (designated as soil category A according Eurocode 8 [12]), and subsequently, the same model underwent testing when situated on compacted sand (representing the soil category E found in norm [12]) as it is shown by Figure 1. The structural model was tested under both dry and saturated sand foundation conditions. These experiments took place at the Laboratory for Structures at the Faculty of Civil Engineering, University of Rijeka.

2.1. STRUCTURAL MODEL

The experimental model is constructed of steel frame, consisting of two columns connected by a sturdy foundation and a rigid beam. The columns are welded at their bases to rectangular pipe, which represents the foundation, and at the top, steel plates are combined to form a rigid beam. To simulate the superstructure mass, a rigid beam was employed.

The foundation itself was fashioned from rectangular pipes, characterized by a cross-sectional dimension of 60 x 40 mm and a solid 5 mm wall. The columns were made from steel sheets, measuring 20 mm in width, 2 mm in thickness, and standing at height of 162 mm all shown in Figure 2. The beam was assembled

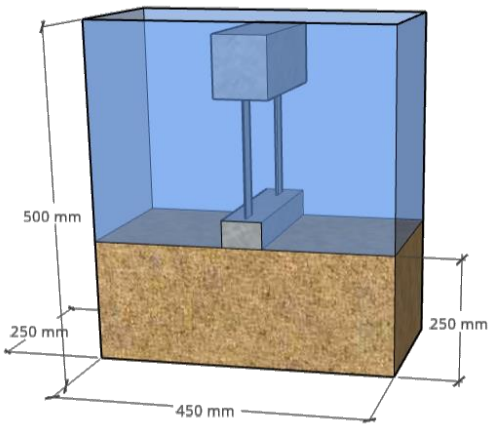

Figure 1. Experimental setup

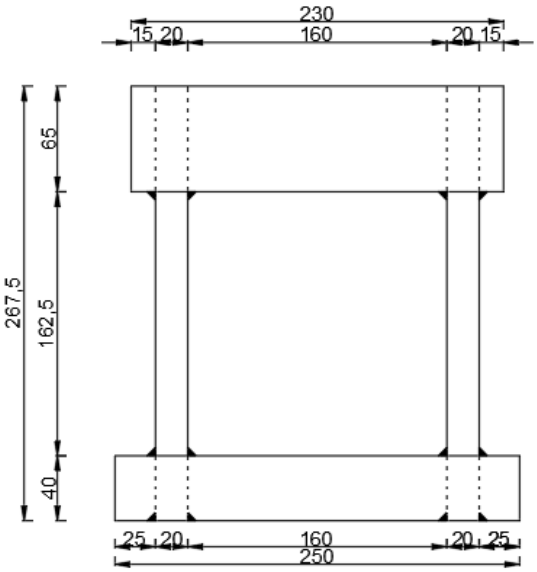

Figure 2. Structural model [dimensions are in mm]

from 10 steel plates, each 65 mm wide and 6 mm thick. Notably, the steel grade utilized in this model was S275. The model as a whole weighted a total of 8.68 kg, with the mass ratio of the upper beam to the foundation beam estimated at roughly 3.5:1. The calculated pressure imposed on the foundation soil by the model was approximately 580 Pa.

2.2. MEASURING INSTRUMENTS

To monitor displacement and acceleration during the experiment, accelerometers were positioned at various key points. These accelerometers were placed on top of the structural model, on the foundation (Figure 4), and on the shaking table platform. Additionally, two optical measuring systems were used to register the displacements accurately.

The GOM Aramis 4M contactless optical 3D system, denoted as "4" in Figure 3, was used to capture the structural model's movements. Simultaneously, the GOM Aramis 12M contactless optical 3D measurement system, identified as "3" in Figure 3, was tasked with tracking soil deformations. This comprehensive approach allowed us to collect data on both the structural response and the changes in the soil during the experiments.

Dynamic response of the structural model was recored at a high frame rate of 160 frames per second, capturing it in full resolution. Dynamic tests were performed by applying dynamic excitation using the Quanser ST-III earthquake platform (marked with number “2” in Figure 3), with ground plan dimensions 70 cm x 70 cm and the possibility of maximum acceleration of

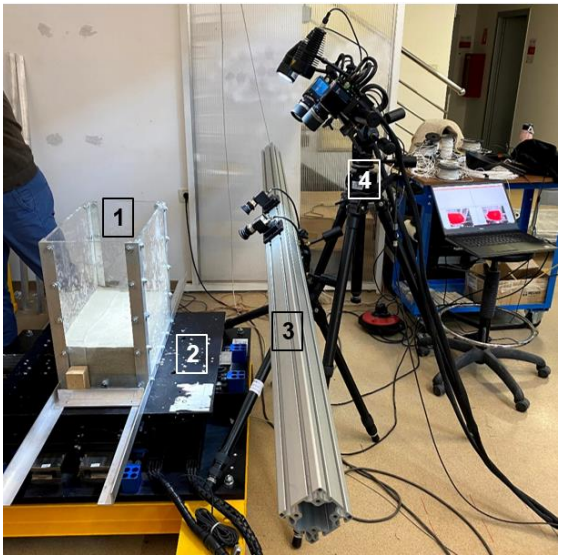

Figure 3. Experimental setup

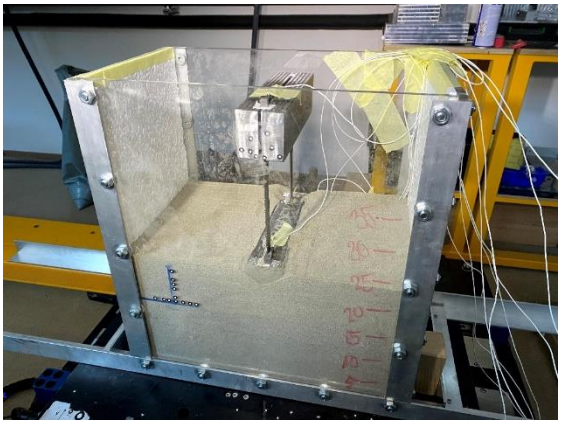

Figure 4. Experimental model with measuring instruments

1 g in both directions at a maximum load of 120 kg.

2.3. FOUNDATION SOIL

For the preparation of the soil model, local Drava sand was used. The properties of sand can be found in study published by Jagodnik et al [13]. Sand was embeded in the rigid container (marked as 1 in Figure 3) which was made of aluminum profiles that formed the frame for plexiglas. Plexiglas was chosen for the container since it is resonubly light and allowes observation and optical measurement of sand behavior before, during, and after testing. The container was reigidly attached to the shaking table. The total mass of the container was 34,8 kg. Due to the limited load capacity of the shaking table (120 kg), the entire model, together with the container and sand, was prepared in accordance with the scaling recommendations given in [14].

Dry sand was methodically placed in approximately 5 cm thick layers. Following the placement of each layer, the shaking table platform was activated, subjecting it to high-frequency vibrations for a duration of roughly 2 minutes. Prior to embedding each layer into the container, all the sand was carefully weighed to determine its mass. After the compaction process was completed, the volume of the sand was measured. These measurements allowed calculation of the density of the compacted sand. The analysis indicated that the mean density of the sand in the layers was close to 1550 kg/m³.

2.4. EXCITATION

Sinesweep function had been chosen as an excitation to ascertain the fundamental frequencies of the tested cases. Additionally, the Kobe 1995 earthquake record was utilised to excite the models, varying the maximum amplitude (A) from 0.2 mm to 0.4 mm.

Testing sequence began with the models initially attached directly to the shaking table platform. Subsequently, they were placed on a layer of sand embedded within the container. Finally, the tests were repeated using saturated sand. This comprehensive approach allowed exploration of the dynamic response of the model under different conditions.

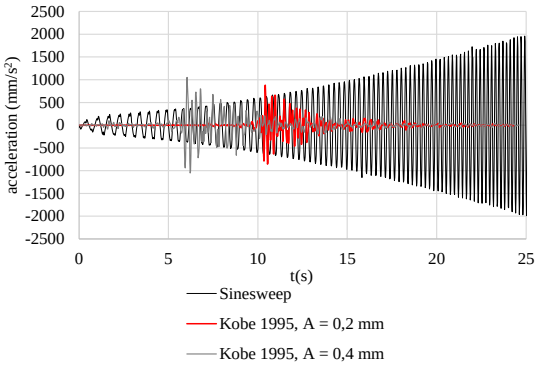

Figure 5. System excitations

3. RESULTS

This chapter presents displacements measured at the top and foundation beam for excitations: Sinesweep function (Figure 6), Kobe earthquake A= 0,2 mm (Figure 7) and lastly, Kobe with an amplitude of A= 0,4 mm (Figure 8). It can be noticed that the displacement of the top beam is smaller for the systems with foundations placed on the sand (Figure 6 (a), Figure 7 (a), Figure 8 (a)). Smaller vibration amplitudes of top beam go in hand with the hypothesis that soil can be observed as isolator/damper in soil-structure systems. Tables 1., 2. and 3. serve as a comparison of experimental research conducted on different foundation conditions. Overall results show higher damping properties when the model is founded on dry sand compared to saturated sand. Exact percentage should be taken conservatively and should be used only as a guideline not a rule.

Results of experimental research conducted on saturated sand are compared to results on dry

Table 1. Top beam displacement ratios for sinesweep function

t(s)	$A/A_{fixed\ base}$	
	Dry sand	Saturated sand
2	99.82%	99.82%
4	74.28%	99.78%
6	13.24%	14.29%
8	12.28%	5.85%
10	9.39%	6.87%
12	7.83%	6.96%
Average	36.14%	38.93%

Table 2. Top beam displacement ratios for Kobe 1995 A=0,2 mm

t(s)	$A/A_{fixed\ base}$	
	Dry sand	Saturated sand
11	112.50%	120.83%
13	62.35%	71.88%
15	68.33%	85.00%
17	76.92%	95.02%
19	47.06%	76.47%
Average	73.43%	89.84%

Table 3. Top beam displacement ratios for Kobe 1995 A=0,4 mm

t(s)	$A/A_{fixed\ base}$	
	Dry sand	Saturated sand
7	17.76%	47.96%
9	21.30%	33.33%
11	5.98%	12.03%
13	4.93%	3.15%
15	9.62%	34.62%
Average	11.91%	26.22%

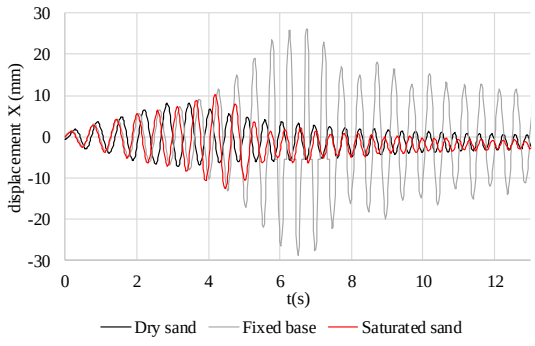

(a) Top beam

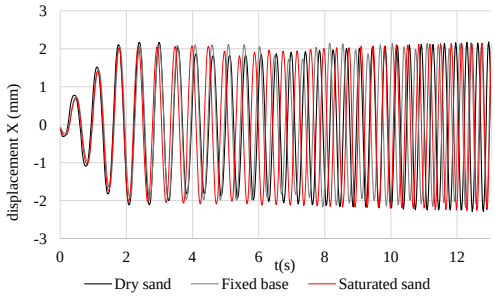

(b) Foundation strip

Figure 6. Structural response for sinesweep function

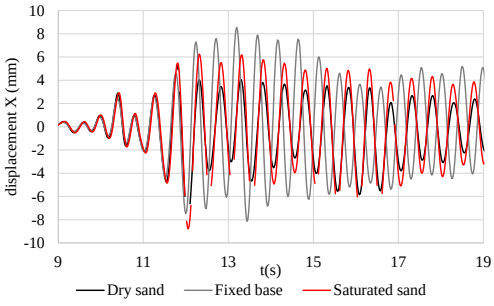

(a) Top beam

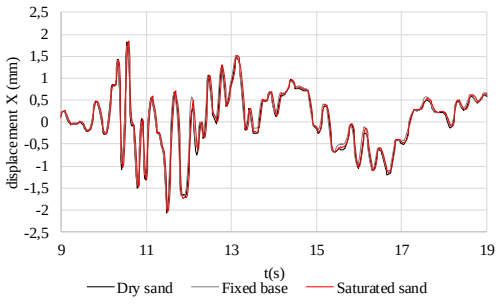

(b) Foundation strip

Figure 7. Model vibration excited by Kobe 1995 A=0,2 mm

sand. It is observed that the soil effects are less noticeable in the case where the sand was saturated. Saturated sand is stiffer compared to dry sand which means that the saturated sand case behaves similar to fixed base condition.

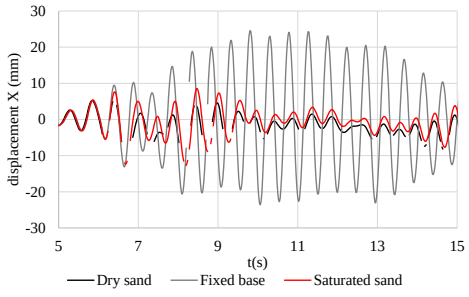

(a) Top beam

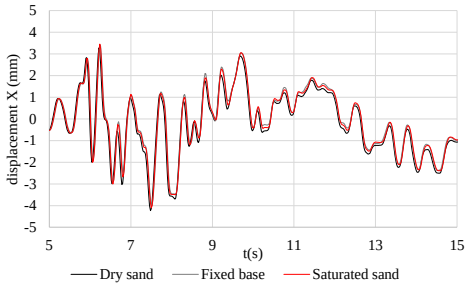

(b) Foundation strip

Figure 8. Model vibration excited by Kobe 1995 A=0,4 mm

Vibrations of the foundation strip are presented in Figure 6 (b), Figure 7 (b) and Figure 8 (b).

When comparing the fixed base condition to the dry and saturated sand case it is noticeable that no major slippage occurred at foundation level. This was concluded since the foundation vibrations measured on sand are almost identical to displacements measured for the fixed base case.

4. CONCLUSION

Dynamic soil-structure interaction experiments are very useful because they bring valuable insights into the behaviour of structures and the soil. The soil-structure interaction effects are still investigated by many to determine the contribution of the soil in the seismic behaviour of soil-structure systems. Small-scale experimental research was conducted using earthquake platform to simulate real excitation. Steel frame model was tested with fixed base and but also founded on sand. A local river sand in dry and saturated conditions was used to simulate the soil. The model vibrations were measured at the top of the model and at the foundation level for three different excitations. It is noticeable that horizontal vibrations for models tested on sand are lower when compared to the fixed base case which could lead to conclusion that compliant soil can be observed as an isolator. Further, horizontal

vibrations measured at the foundation level showed no significant slippage happening at the foundation level.

The main goal of the research was to investigate the impact of foundation soil flexibility on seismic behaviour of structures with shallow foundations through original experimental research on small-scale model. Analyzing the results one can conclude that fixed base models have different behaviour compared to models founded on soil. Further, stiffness of the soil has a big impact on the behaviour of the soil-structure system where stiffer foundation soil results with behaviour closer to fixed base case while the flexible soil changes behaviour of the models considering the displacements which are the result of dynamic excitation. Precisely, when sinesweep excitement was observed, dry sand resulted with average of 36% and saturated sand with 39% of top beam displacements of the fixed base case. Kobe 1995 A=0,2 cm excitement showed 73% and 89% of top beam displacements for dry and saturated sand while Kobe 1995 A=0,4cm showed much higher damping properties where dry sand had 12% and saturated sand 26% od fixed base case top beam displacements. One can conclude that damping properties have higher impact when stronger excitement was used, yet it needs to be taken into account that tests where done in following order: sinesweep, Kobe 1995 A=0,2 cm and Kobe 1995 A=0,4 cm which results in changes in the soil properties as the tests went on.

Although certain conclusions can be drawn, extended experimental research and thorough numerical modeling could provide better understanding of the effects in the soil and confirm results presented within this paper.

Acknowledgements

This study was carried out within the framework of the project SYNERGY and financially supported by the Faculty of Civil Engineering and Architecture Osijek.

REFERENCES

[1] Anastasopoulos, I.: 'Beyond conventional capacity design: towards a new design philosophy', Soil–foundation–structure interaction. New York: CRC Press, Taylor & Francis Group, 2010, pp. 213-220.

[2] Pender, M., Algie, T., Orense, R., Wotherspoon, L., and Sa'Don, N.: 'Snap-back testing for estimation of nonlinear behaviour of shallow and pile foundations', in Editor: 'Book Snap-back testing for estimation of nonlinear behaviour of shallow and pile foundations' (2011, edn.), pp.

[3] Kumar, M., and Mishra, S.: 'Study of seismic response characteristics of building frame models using shake table test and considering soil–structure interaction', Asian Journal of Civil Engineering, 2019, 20, (3), pp. 409-419.

[4] Prevost, J.H., and Scanlan, R.H.: 'Dynamic soil-structure interaction: centrifugal modeling', International Journal of Soil Dynamics and Earthquake Engineering, 1983, 2, (4), pp. 212-221.

[5] Knappett, J., Haigh, S.K., and Madabhushi, S.G.: 'Mechanisms of failure for shallow foundations under earthquake loading', Soil Dynamics and Earthquake Engineering, 2006, 26, (2-4), pp. 91-102.

[6] Pender, M., Algie, T., Storie, L., and Salimath, R.: 'Rocking controlled design of shallow foundations', in Editor (Ed.)^(Eds.): 'Book Rocking controlled design of shallow foundations' (2013, edn.), pp.

[7] Abate, G., and Massimino, M.R.: 'Dynamic soil-structure interaction analysis by experimental and numerical modelling', Riv Ital Geotecn, 2016, 50, (2), pp. 44-70.

[8] Martakis, P., Taeseri, D., Chatzi, E., and Laue, J.: 'A centrifuge-based experimental verification of Soil-Structure Interaction effects', Soil Dynamics and Earthquake Engineering, 2017, 103, pp. 1-14.

[9] Hirave, V., and Kalyanshetti, M.: 'Seismic response of steel braced building frame considering soil structure interaction (SSI): an experimental study', Journal of the Institution of Engineers (India): Series A, 2018, 99, (1), pp. 113-122.

[10] Anastasopoulos, I., Kourkoulis, R., Gelagoti, F., and Papadopoulos, E.: 'Rocking response of SDOF systems on shallow improved sand: An experimental study', Soil Dynamics and Earthquake Engineering, 2012, 40, pp. 15-33.

[11] Lee, M., Bae, K.-T., Lee, I.-W., and Yoo, M.: 'Cyclic py curves of monopiles in dense dry sand using centrifuge model tests', Applied Sciences, 2019, 9, (8), pp. 1641.

[12] CEN. 2005a. Eurocode 8: Design of structures for earthquake resistance - part 1: General rules, seismic actions and rules for buildings, design code EN 1998-1. Brussels, Belgium: European Committee for Standardisation.

[13] Jagodnik, V., Kraus, I., Ivanda, S., and Arbanas, Ž.: 'Behaviour of Uniform Drava River Sand in Drained Condition—A Critical State Approach', Applied Sciences, 2020, 10, (17), pp. 5733.

[14] Harris, H.G., and Sabnis, G.: 'Structural modeling and experimental techniques' (CRC press, 1999. 1999.

Jansun Bukovetz
MD
Institute of Public Health of the Republic of North Macedonia, Skopje
N. Macedonia
cansun-97@hotmail.com

Mihail Kochubovski
MD, PhD, Professor
Institute of Public Health of the Republic of North Macedonia, Skopje
Ss. Cyril and Methodius University in Skopje
Faculty of Medicine
N. Macedonia

Gordana Kaplan
PhD, Professor
Institute of Earth and Space Sciences
Eskisehir Technical University
Turkey

URBAN HEAT ISLAND AND GREEN SPACES IN THE CITY OF SKOPJE: AN ENVIRONMENTAL HEALTH APPROACH COMBINED WITH REMOTE SENSING DATA

The Surface Urban Heat Island (SUHI) is a well-documented urbanization-driven phenomenon, contributing to elevated city temperatures compared to surrounding rural areas. This study investigates the positive impact of green spaces in alleviating ambient temperatures during Skopje's summer. Conducted from July 22 to July 28, 2022, in Skopje, Republic of North Macedonia, our cross-sectional research involved thrice-daily temperature monitoring across various locations with and without tree coverage. Additionally, leveraging Landsat-8 data from July 22, 2022, we extracted and analyzed SUHI patterns.

Among the nine locations studied, four exhibited clear Urban Heat Island (UHI) effects. The most significant temperature disparity of 7.9°C was observed between a treeless one-way street and the City Park. On average, temperature differences between the hottest and coolest spots amounted to 6.8°C, consistently showcasing lower ambient temperatures in tree-covered areas.

Our findings underscore the pivotal role of green spaces, including parks and tree-lined gardens, in mitigating thermal stress and offsetting the adverse impacts of UHI on public health. This study emphasizes the critical importance of urban planning strategies that prioritize and integrate green infrastructure to address the challenges posed by UHI, urbanization, and climate change. Policies aimed at promoting and preserving green spaces are indispensable for fostering climate-resilient and sustainable cities that prioritize the well-being of their inhabitants.

Keywords: Urban Heat Island, Green Spaces, Landsat-8, LST, NDVI

INTRODUCTION

Urban environments are amidst an unprecedented era of transformation, driven by rapid urbanization and the omnipresent specter of climate change. In this context,

understanding and addressing urban heat islands (UHIs) emerge as a pivotal concern for contemporary urban planners, policy-makers, and public health experts (Gabriel & Endlicher, 2011; Luber & McGeehin, 2008). This phenomenon, fueled by population growth and increasing industrialization, has resulted in the proliferation of cities and urban areas worldwide. However, this unprecedented urban sprawl has not come without consequences (Chatterjee & Majumdar, 2022). Surface Urban Heat Island (SUHI) is a phenomenon in which urban areas experience higher temperatures than their surrounding rural areas due to human activities such as industrialization, urbanization, and transportation (Almeida et al., 2021). This is caused by the modification of the land surface in urban areas, which leads to changes in the energy balance and creates a positive heat flux. The land surface modifications in urban areas, such as replacing vegetation with impervious surfaces like concrete and asphalt, result in changes to the surface properties that can trap and store heat (Ngie et al., 2014). Human activities such as energy consumption, transportation, and industrial activities can also generate heat that adds to the heat island effect. SUHI has a wide range of negative impacts, including increased energy consumption, higher cooling costs, reduced air quality, and negative impacts on human health. Mitigation strategies for SUHI include promoting green spaces and urban vegetation, green roofs, cool roofs, reflective pavements, and smart urban design incorporating natural ventilation and shading to reduce heat absorption. Insufficient soil volumes and soil compaction (Jim, 2019), increased air pollution (Chen et al., 2015) and high temperatures with their water stress effect (Meineke et al., 2016) undoubtedly may negatively affect growth of trees and their shading cooling effect. In addition, canopy size (Rahman et al, 2015), shape (McPherson et al., 2018), and structure (Smithers et al., 2018) are the other morphological characteristics that affect the tree shading. The vegetation absorbs solar energy and provides shade, which lowers the temperature of the ground and increases the latent heat exchange for evapotranspiration. The most important factor in UHI mitigation and adaptation is urban vegetation. Trees could lower daytime air temperatures by up to 2°C at 60 m above ground level and 4°C at the tree level (4 m above ground) (Wang & Akbari, 2016). It has been demonstrated that the effect of transpiration on air temperatures varies between 1° and 8°C (Rahman et al, 2017) or between 2°C to 8°C (Taha, 1997). In addition, according to Turner-Skoff, vegetation has a significant cooling effect in cities, lowering air temperatures by 0.5° to 9°C (Turner-Skoff & Cavender, 2019) and all of these are in line with our measured temperatures. Recent studies investigates the relationship between the land cover and thermal response (Fuladlu, 2022), LST and major air pollutants (Fuladlu and Altan, 2021), air quality and SUHI intensity (Alqasemi, Abduldaem S., et al, 2021).

While extant literature offers valuable insights into UHIs, our manuscript aspires to transcend the limitations of existing knowledge by offering novel perspectives on the intricate interplay between urban development, climate change, and the specific dynamics of UHI within the context of Skopje (Kaplan et al., 2019; Coutts et al., 2007). Departing from mere replication, our study embarks on uncharted paths by harnessing empirical data, in-situ measurements, and historical remote sensing analyses. This ambitious endeavor endeavors not only to unravel immediate UHI impacts but also to trace the historical trajectories that underpin these phenomena (Rahman et al., 2017; Wang & Akbari, 2016; Kocubovski et al., 2023).

Remote sensing techniques and urban climate models can also be used to monitor and understand the extent, causes of SUHI, and inform effective mitigation strategies (Despini et al., 2021). Land Surface Temperature (LST) refers to the temperature of the Earth's surface, as measured by remote sensing instruments or ground-based sensors. It is an important variable in climate studies and environmental monitoring, as it provides information on the energy exchange between the land surface and the atmosphere. LST can be estimated using thermal infrared (TIR) remote sensing data, which measures the thermal radiation emitted by the Earth's surface (Avdan & Jovanovska, 2016).

Remote sensing data unveils trends in Urban Heat Island (UHI) development within Skopje. Generally, higher Normalized Difference Vegetation Index (NDVI) values correspond to lower Land Surface Temperature (LST) due to vegetation's cooling effect through transpiration and photosynthesis (Chen et al., 2006). Conversely, lower NDVI areas like urban spaces tend to exhibit higher LST, reflecting increased heat absorption (Tao et al., 2020). Our study employs remote sensing techniques (Avdan & Jovanovska, 2016) alongside NDVI (Meili et al., 2021; Rahman et al., 2015) and urban climate models (Despini et al., 2021) to comprehend and address Surface Urban Heat Islands (SUHIs). Although the NDVI-LST

relationship is context-dependent (Li et al., 2009), combining these data provides insights into land surface processes and UHI hotspots (Meili et al., 2021; Rahman et al., 2015). In-situ measurements corroborate the negative correlation between LST and NDVI, highlighting vegetation's pivotal role in mitigating UHI effects (McDonald et al., 2021; Steensen et al., 2022; Despini et al., 2021).Surface urban heat islands (SUHIs) differ from atmospheric UHI in that they are determined by the temperature of the entire 3-D surface envelope rather than just the air temperature differences between urban and rural areas. SUHIs are present both day and night but are strongest during the day when the sun is shining and heat is accumulating in cities. The loss of natural cooling effect due to the replacement of green areas with man-made structures causes built-up areas to release heat at night (Tomlinson et al., 2011). Factors, such as the type and density of buildings, surface materials, and meteorological conditions, can also influence UHI and LST.

This study represents an effort to transcend superficial observations, delving deeper into unraveling intricate patterns and changes in UHIs within Skopje. Employing a strategic blend of geospatial data and empirical evidence, our study seeks to deviate from conventional methodologies, exploring innovative approaches to comprehend and effectively manage UHIs. By providing actionable intelligence for sustainable urban development, our study endeavors to create a foundation for informed decision-making amidst an evolving climate landscape (McDonald et al., 2021; Meili et al., 2021). Through the integration of remote sensing satellite data and in-situ measurements, our study will facilitate the analysis of air temperature, derive NDVI and LST, and extract UHI areas from Landsat-8 data, enabling comprehensive comparative analysis.

The aim of the study is to combine in-situ (field-based) measurements with remote sensing data, providing a comprehensive analysis that bridges the gap between on-ground observations and broader spatial patterns of UHI in Skopje, and to reveal the differencies in ambient air temperatures between the streets with and without tree line during the heat waves in Skopje.

MATERIALS AND METHODS

STUDY AREA

The City of Skopje is situated in the central part of the Skopje valley 42°0′N 21°26′E, altitude 240 m and covering an area of 571,46 km^2. According to Census 2021 data, the population is 526,502 and urban density 1,400/km^2. The region's relief is complex, comprised of a valley and surrounding mountains on the northwest and on the south, and east. The main direction of the valley is from the northwest to the southeast, being shaped by the action of the river Vardar. Mostly the valley is under the influence of a Continental and Mediterranean type of climate, as well as under the influence of a mountain climate at higher elevations. Lower parts of the valley experience hot and dry summer periods and moderately cold and wet winters (Kaplan et al., 2018; Kendrovski, 2006). The valley's average annual air temperature is 12.9 °C, with an upward trend from 1978 to 2015. The last ten years have seen the most frequent short heat waves, which can last up to six days. The total annual precipitation is 484.8 mm on average. Long dry periods in the summer are a result of the irregular spatial and temporal distribution of precipitation (Donevska & Panov, 2019). The summers are long, hot and relatively dry with low humidity. Skopje's average July high is 31°C. On average Skopje has 88 days above 30°C each year, and 10.2 days above 35.0°C every year. The threshold temperature for heat wave in July in Skopje is 37.0°C according to three decades of air temperature measurements. The Heat-Health Action Plan to prevent consequences on the population's health in the Republic of Macedonia was adopted in 2011, and the threshold ambient air temperatures for Skopje have been used for the study we performed in July 2022. The Heat-Health Action Plan has been developed to implement adaptation measures and prevent health consequences of extreme heat caused by changing weather conditions as a result of the climate change (WHO, 2014).

IN-SITU MEASUREMENTS

During the 2022 heat wave in Skopje, Republic of North Macedonia, the cross-sectional study was conducted from July 22nd to July 28th, excluding July 28th when the heat wave had subsided. Six locations for temperature measurements across the day and an additional three locations were selected for midday measurements. To conduct these measurements, we opted for an eco-friendly mode of transport—bicycles. During the study

our field measurements were compared with measured temperatures from both the Hydrometeorological Service of the Republic of North Macedonia and AccuWeather.

Measurements of the ambient air temperature were performed three times daily: in the morning (6 a.m. to 8 a.m.), midday (1:30 p.m. to 4:30 p.m.), and evening (9 p.m. to 11 p.m.). Specific boulevards and streets in Skopje have been selected - such as Saint Clement of Ohrid, Ilinden, Boris Trajkovski, Partizanski odredi, Nikola Trimpare, and Kosturski heroi—to compare temperatures with and without tree lines. Based on the Regulation for Urban Planning (Ministry of Transport and Communications, 2022), and it were noted differences in traffic lane widths, ranging from 3.25-3.75 meters.

Midday measurements included pedestrian refuge islands on main streets without tree cover (boulevard Ilinden and boulevard Saint Clement of Ohrid) and Skopje City Park, where tree lines are typically comprised of lime trees with medium or large canopies.

For the measurements, we used a calibrated thermometer that adhered to quality assurance guidelines accredited as per MKC EN ISO/IEC 17025:2018, calibrated on May 19th, 2022. The thermometer had a maximal registered measurement error of -0.3°C, with an allowed tolerance of ±0.6°C. The measurement uncertainty was calculated using EA-4/02 M:2022, with a coverage factor k=2, providing a 95% probability that the true value falls within the corresponding interval. The thermometer was placed at a height of 1.5 meters from the ground and it took 15 minutes to show the results. We sourced relative humidity data from AccuWeather (AccuWeather, 2022).

REMOTE SENSING DATA

In order to extract SUHI from satellite data, we used Landsat-8 data from 22 July, 2022. As the temporal resolution of Landsat-8 is 16 days, this date was the only available data within the in-situ measurement date. One of the key products of Landsat-8 is LST, which is derived from thermal infrared imagery acquired by the satellite's Thermal Infrared Sensor (TIRS).

LST is important in many Earth system science applications, including climate modeling, agriculture, hydrology, and urban planning. The TIRS instrument on Landsat-8 provides two thermal bands used to estimate LST. The algorithm used to calculate LST from TIRS data considers atmospheric effects, such as water vapor and aerosols, which can affect the accuracy of the LST estimates.

To calculate LST from Landsat-8, several LST algorithms have been developed over the years. In this study, we used the algorithm developed by (Avdan &Jovanovska, 2018). We added 100-m buffer around each air-temperature measuring point to better understand the in-situ points' surroundings.

From the LST data, SUHI was calculated from remote sensing data using the following equation:

$$SUHI = \mu + \frac{\sigma}{2}$$

where μ is the mean LST value of the study area and σ is the standard deviation of the LST. Areas that have higher temperature values than the SUHI are considered areas highly affected by the UHI phenomenon.

To investigate the relation between SUHI, LST, air temperature and vegetation cover, we also calculated NDVI from the Landsat-8 data (Figure 2). NDVI is a widely used vegetation index that provides a quantitative measure of the amount of green vegetation in a particular area. It is based on the principle that healthy vegetation absorbs most of the visible light (i.e., blue, green, and red) and reflects much of the near-infrared (NIR) light. The NDVI is calculated by dividing the difference between the NIR and red bands' reflectance values by their sum. The resulting index ranges from -1 to 1, with values closer to 1 indicating a high vegetation density and values closer to -1 indicating a low vegetation density or non-vegetation areas. NDVI is commonly used in remote sensing applications to monitor vegetation density changes over time, detect and map land cover changes, and estimate biophysical parameters related to vegetation, such as leaf area index, biomass, and productivity.

ANALYSIS & RESULTS

The obtained measurements in our study showed the influence of the green spaces on the air temperature in the city of Skopje during the heat wave and one day later. In four tables we present the temperature difference in different periods of day i.e. on morning, midday and evening relative humidity.

Graph 1 illustrates the average ambient air temperature difference between the measuring

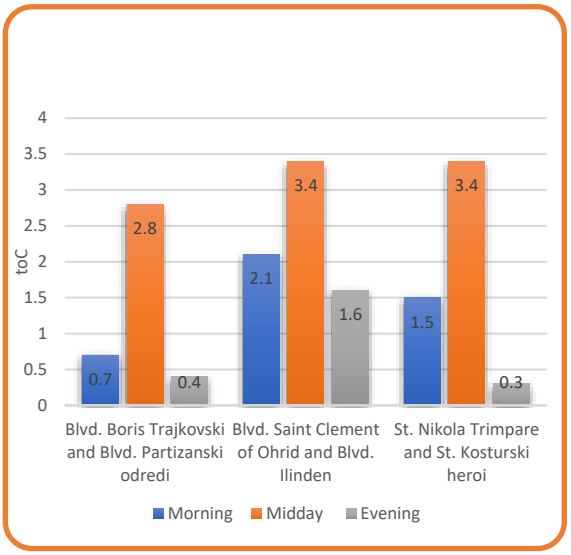

Graph 1. Temperature difference in the morning, at midday and in the evening on the investigated sites presenting the temperature differences between selected streets and boulevards

sites and the biggest difference was registered at midday and the lowest in the evening.

Table 1. Temperature difference in the morning, at midday and in the evening on the investigated sites

Date	Compared locations	Morning temperature difference (T°C)	Midday temperature difference (T°C)	Evening temperature difference (T°C)
22.07.2022	Blvd. Boris Trajkovski and Blvd. Partizanski odredi	1.4	1.1	0.4
23.07.2022		1.7	2.3	0.9
24.07.2022		0.7	2	0.7
25.07.2022		0.2	3.5	0
26.07.2022		0.2	1.8	0.2
27.07.2022		0.1	4.1	0.4
28.07.2022		0.8	4.8	0.3
Average T°C		**0.7**	**2.8**	**0.4**
Date				
22.07.2022	Blvd. Saint Clement of Ohrid and Blvd. Ilinden	1.8	3.1	3
23.07.2022		2.5	2	1.4
24.07.2022		2.1	4.1	2.1
25.07.2022		1,9	3,3	1,1
26.07.2022		2.3	4.3	2
27.07.2022		1.7	3.2	1.1
28.07.2022		2.6	4	0.2
Average T°C		**2.1**	**3.4**	**1.6**
Date				
22.07.2022	St. Nikola Trimpare and St. Kosturski heroi	1.7	2.6	0.5
23.07.2022		1.8	2.5	0
24.07.2022		1.7	3.8	0.2
25.07.2022		2.6	5.3	0.1
26.07.2022		1.7	5.2	0.4
27.07.2022		0.4	3	0.5
28.07.2022		0.6	1.5	0.7
Average T°C		**1.5**	**3.4**	**0.3**

Compared locations	Average morning temperature difference (T°C)	Average midday temperature difference (T°C)	Average evening temperature difference (T°C)
Blvd. Boris Trajkovski and Blvd. Partizanski odredi	0.7	2.8	0.4
Blvd. Saint Clement of Ohrid and Blvd. Ilinden	2.1	3.4	1.6
St. Nikola Trimpare and St. Kosturski heroi	1.5	3.4	0.3
Average T°C	**1.4**	**3.2**	**0.8**

From the obtained measurements of morning, midday and evening temperatures, it can be seen that the highest temperature range was registered on the measuring sites on Blvd. Saint Clement of Ohrid and Blvd. Ilinden in the morning and in the evening, compared to other locations.

Table 2. Morning, midday and evening temperature range

Date	Compared locations	Morning temperature range (T°C)	Midday temperature range (T°C)	Evening temperature range (T°C)
22.07.2022 – 28.07.2022	Blvd. Boris Trajkovski and Blvd. Partizanski odredi	0.1 - 1.7	1.1 - 4.8	0 - 0.9
	Blvd. Saint Clement of Ohrid and Blvd. Ilinden	1.7 - 2.6	2 - 4.3	0.2 – 3
	St. Nikola Trimpare and St. Kosturski heroi	0.4 - 2.6	1.5 - 5.3	0 - 0.7

The highest air temperature was registered on a pedestrian island on Blvd. Saint Clement of Ohrid. This was expected, as there are more trees on Boulevard Ilinden. The positive impact of the greenery is obvious.

Table 3. Air temperature on extra three locations for midday measurements

Date	Temperature on pedestrian refuge island on boulevard Ilinden (T°C)	Temperature on pedestrian refuge island on boulevard Saint Clement of Ohrid (T°C)	Skopje City Park (T°C)
22.07.2022	37.3	39.5	32.4
23.07.2022	38.1	38.9	33.4
24.07.2022	41.4	42	35.7
25.07.2022	38	39.4	32
26.07.2022	40.5	40.1	34.2
27.07.2022	38.1	36	33.3
28.07.2022	33.9	32.4	29.3
Average T°C	38.2	38.3	32.9

Skopje City Park was the coolest area among the measured places in 6 from 7 days (Table 4).

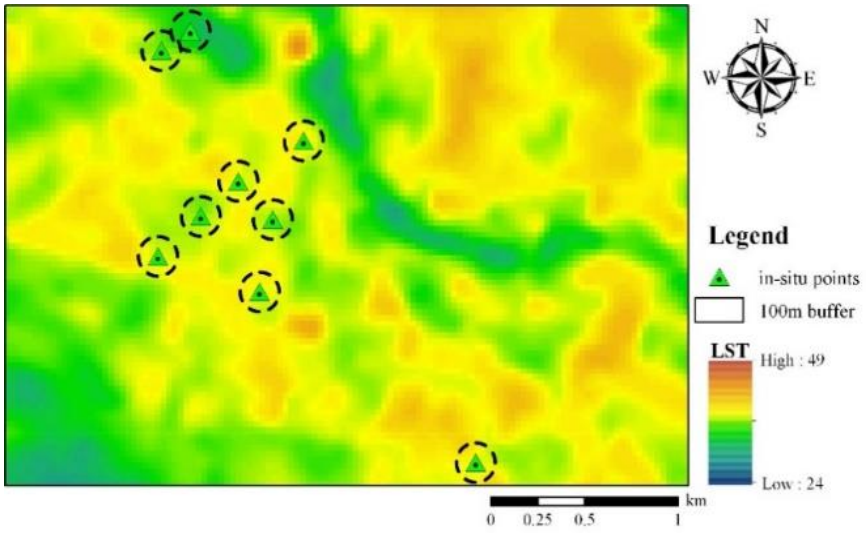

Figure 1. LST map in the study area

Table 4. The highest air temperature difference between the hottest and coolest measured areas at midday

Date	Areas with the highest temperature difference	T°C
22.07.2022	Pedestrian refuge island on boulevard Saint Clement of Ohrid and Skopje City Park	7.1
23.07.2022	St. Nikola Trimpare and Skopje City Park	6.2
24.07.2022	Pedestrian refuge island on Boulevard Saint Clement of Ohrid and Boulevard Partizanski odredi	7
25.07.2022	Pedestrian refuge island on boulevard Saint Clement of Ohrid and Skopje City Park	7.4
26.07.2022	St. Nikola Trimpare and Skopje City Park	7.9
27.07.2022	Pedestrian refuge island on boulevard Ilinden and Skopje City Park	5
28.07.2022	Blvd. Boris Trajkovski and Skopje City Park	7.2
Average T°C		**6.8**

RESULTS FROM THE REMOTE SENSING DATA

The recorded LST in the study area ranged from 24°C to 49°C, as depicted in Figure 1. On July 26th, 2022, the mean LST was 33.3°C, with a standard deviation of 2.9°C. Areas with temperatures surpassing 34.75°C were identified as being impacted by Surface Urban Heat Island (SUHI) effects. These findings guided our geospatial analysis to pinpoint UHI-affected zones, showcased in Figure 3.

To investigate the immediate surroundings, we conducted geospatial statistical analysis within 100-meter buffer zones, extracting NDVI values (Figure 2) and examining their impact on SUHI. Table 6 illustrates the NDVI values from this analysis, indicating whether specific locations

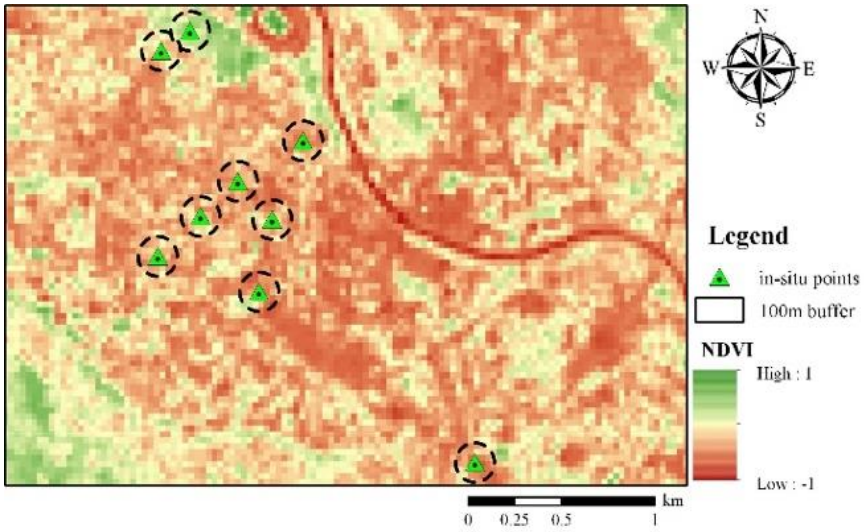

Figure 2. NDVI map in the study area

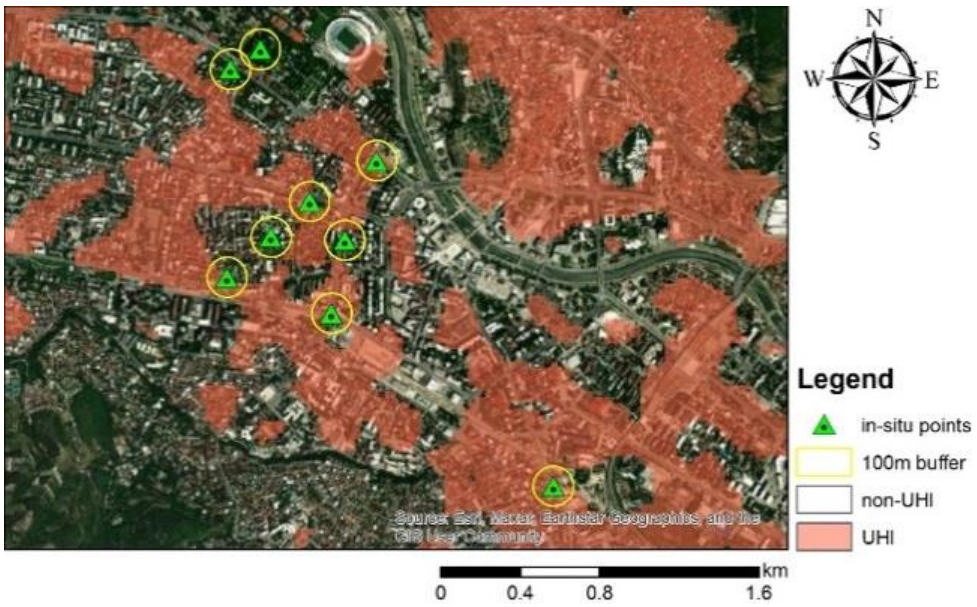

Figure 3. UHI-affected areas in the study area

Table 5 NDVI values in the in-situ locations and buffer zones

ID	1 Pedestrian refuge island on Blvd. Ilinden	2 Blv. Boris Trajkovski	3 Pedestrian refuge island on Blvd. Clement of Ohrid	4 St. Kosturski heroi	5 St. Nikola Trimpare	6 Blvd Partizanski odredi	7 Skopje City Park	8 Blvd Ilinden	9 Blvd Saint Clement of Ohrid
point	0.05	0.05	0.08	0.2	0.23	0.1	0.37	0.24	0.21
100 m min	0.05	0.03	0.02	0.07	0.08	0.07	0.19	0.09	0.06
100 m max	0.26	0.26	0.34	0.28	0.28	0.22	0.44	0.35	0.32
100 m mean	0.13	0.13	0.13	0.17	0.18	0.15	0.36	0.22	0.17
100 m sum	4.5	5	4.5	6	6.33	5.1	12	7.9	6
UHI	YES	YES	YES	NO	NO	YES	NO	NO	NO

Table 6 LST (land surface temperature) in Skopje on 26 July 2022

ID	1 Pedestrian refuge island on Blvd. Ilinden	2 Blv. Boris Trajkovski	3 Pedestrian refuge island on Blvd. Clement of Ohrid	4 St. Kosturski heroi	5 St. Nikola Trimpare	6 Blvd Partizanski odredi	7 Skopje City Park	8 Blvd Ilinden	9 Blvd Saint Clement of Ohrid
point	35.1	34.5	34.7	34.3	33.6	34.5	30.4	33.3	33.8
100 m min	33.7	34.03	34.1	33.7	33	34.16	29.8	31.7	33
100 m max	35.2	36.7	35.1	35.1	34.26	35.3	31.9	34.2	34.8
100 m mean	34.6	34.7	34.7	34.4	33.6	34.6	30.9	33.26	34
UHI	YES	YES	YES	NO	NO	YES	NO	NO	NO

were affected by SUHI according to Figure 3. Locations with NDVI values below 0.2 were identified as SUHI-affected areas. Furthermore, a total NDVI value below six indicated UHI impact, highlighting the vegetation cover's influence on UHI occurrence.

Table 7 showcases the results of the similar geospatial statistical analysis for LST data, correlating areas with temperatures exceeding 34.5°C to UHI-affected regions. It's evident that substantial portions of Skopje were impacted by UHI, with four out of nine in-situ locations experiencing these effects.

A strong negative correlation (R = -0.90) between LST and NDVI values (Figure 4) was observed. This correlation aligns with expectations, where higher NDVI values (indicating greater vegetation cover) correlated with lower LST values. Conversely, lower NDVI values (reflecting limited vegetation cover) corresponded to higher LST values. This relationship underscores the role of vegetation in mitigating heat by providing shade and transpiration, which reduces land surface temperatures. The observed correlation between LST and NDVI values serves as a valuable tool for monitoring land surface

conditions and identifying areas prone to environmental stress. Areas with low vegetation cover exhibited higher temperatures, highlighting the significance of vegetation in moderating UHI effects. This understanding aids in tracking changes in land surface conditions and identifying areas susceptible to environmental impacts.

Urbanization has significantly influenced temperature shifts, evidenced by our comparative analysis of meteorological data between 2009 and 2019. Notably, we observed drastic increases in average temperatures from 20°C to 30°C, with maximum temperatures escalating from 27°C to 32°C during this period. These trends underscore a concerning association between urban expansion and escalating temperatures within our study area.

Remote sensing data unveiled a compelling correlation (R2 = 84) between the UHI and built-up areas, elucidating the dominant role of human activities in driving the UHI

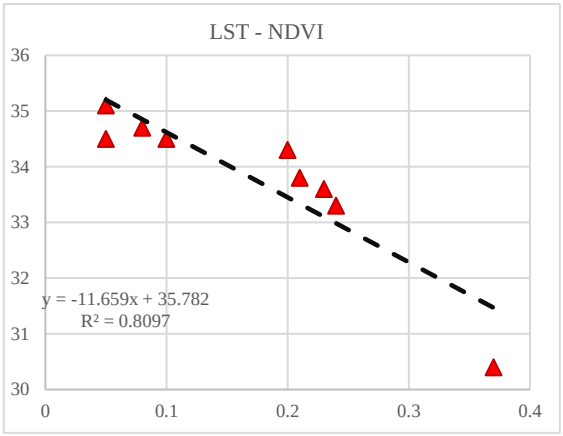

Figure 4. Correlation between NDVI and LST values from satellite data

phenomenon within our study locale. Moreover, an equally compelling correlation (R2 = 90) emerged between verdant spaces and areas unaffected by UHI, illuminating the substantial mitigation potential of green canopies in combatting UHI and SUHI effects, echoing previous findings (Kaplan, 2019). Vegetative

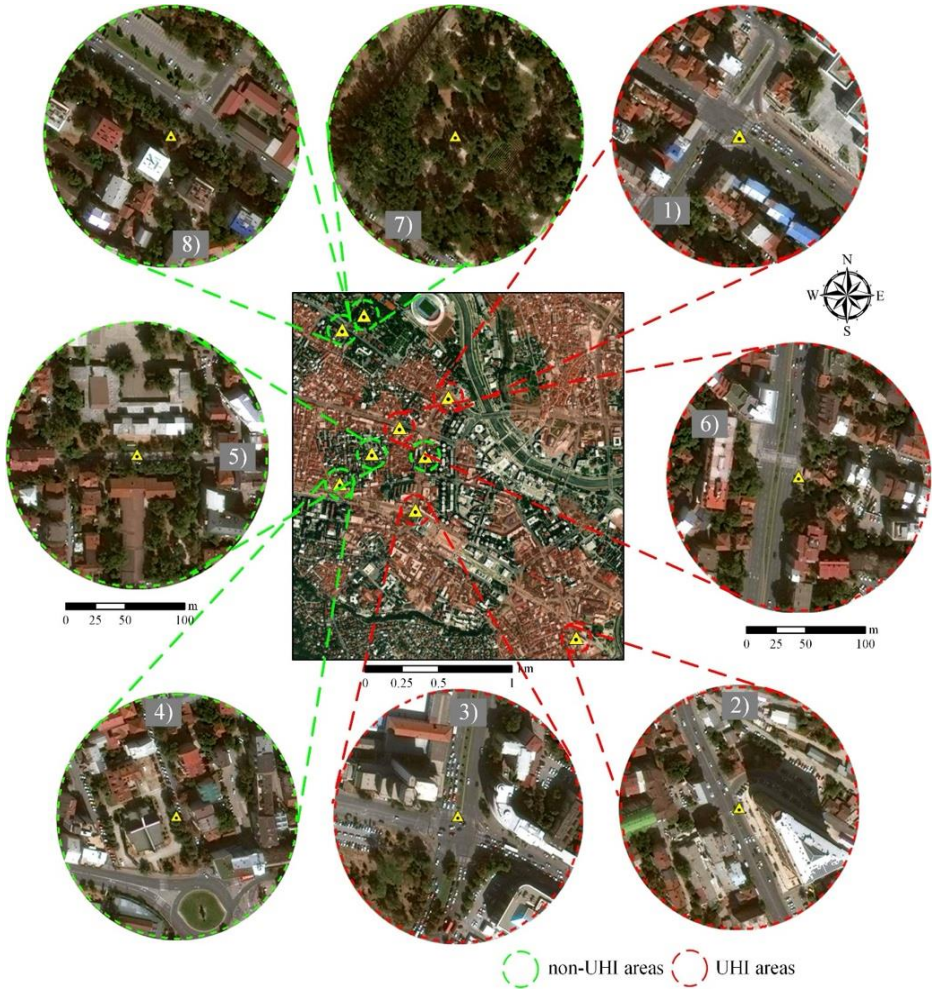

Figure 5. Detailed visualization of the 100-m buffers of the in-situ measurements; 1) Pedestrian refuge islands on Blvd. Ilinden; 2) Blvd. Boris Trajkovski; 3) Pedestrian refuge islands on Blvd. Saint Clement of Ohrid; 4) St. Kosturski heroi; 5) St. Niko

elements, including shrubs, trees, and urban forests, collectively known as biomass, exhibited a pronounced ability to ameliorate UHI effects. Their presence fosters critical processes like evapotranspiration and enhanced water absorption, thus nurturing a microclimate that curbs the adverse impacts of climate change, such as floods and localized atmospheric heating (Coutts et al., 2007).

Our findings align harmoniously with established literature, notably highlighting the substantial temperature differences observed during different times of the day. Morning-to-evening disparities of 0.6°C were detected between locations with and without trees, showcasing the cooling influence of vegetation. Most significantly, boulevards consistently exhibited the widest temperature differentials, irrespective of the time of measurement. Notably, the most extensive temperature range appeared between St. Nikola Trimpare and St. Kosturski heroi during morning and noon measurements, while evening measurements recorded the broadest range between boulevards. Intriguingly, pedestrian islands consistently exhibited equal or higher temperatures compared to the boulevards linking them, potentially influenced by slight delays at exit points, leading to heightened perceived temperatures.

The combined influences of evapotranspiration, shading, and the albedo effects of trees represent a triumvirate of factors shaping the urban climate (Schwaab et al., 2021). Characteristics such as tree height, canopy spread, and leaf density significantly contribute to the benefits trees offer. Notably, a mere 10% increase in tree cover demonstrated a substantial reduction in air temperatures by 3-4°C. This reduction not only curtails energy consumption but also yields consequential benefits such as decreased reliance on fossil fuels (Elmqvist et al., 2015). In our study, we recorded air temperature decreases of 3-4°C in streets and boulevards, both with and without tree lines, showcasing the substantial cooling potential of urban greenery. The average midday temperature difference notably stood at 3.2°C, affirming the cooling effect offered by vegetative cover during peak daytime temperatures.

Morphofunctional features of trees and the urban area circumstances have an impact on the level of transpiration and their cooling effect. The cooling effects via evapotranspiration are an undeniable fact confirmed by a series of scientific studies (Oke, 1988). There is a dilemma in climate projections about the impact of CO_2 concentrations (Sperry et al., 2019).

Temperature variations between the hottest and coolest areas of our study exhibited a substantial difference, with the largest reaching 7.9°C—from a treeless Nikola Trimpare street (42°C) to Skopje's City Park (34.1°C). Our findings echoed similar studies in various cities (Meili et al., 2021), showcasing that cooling effects are notably pronounced during summer afternoons.

Studies in different locations—Madison, Wisconsin (Ziter et al., 2019), Washington DC (Alonzo et al., 2021), and Beijing (Jiao et al., 2017)—highlighted morning cooling ranging from 1°C to 1.8°C, correlating with our observed morning temperature differences of 1.4°C within a range of 0.1-2.2°C. Streets with high tree cover showed a temperature variance of 5.4°C compared to 2.3°C for medium tree-covered streets (Ren et al., 2022). Variability in daytime temperatures within urban landscapes averaged 3.5°C (range, 1.1–5.7°C) (Ziter et al., 2019), aligning with our midday measurements of 3.2°C within a range of 1.1-5.3°C. Notable temperature drops between areas with and without trees were confirmed; streets with high tree canopy covers showed a potential afternoon air temperature reduction of up to 3.3°C (Huang et al., 2020). Nighttime temperatures also displayed a variance of 0.8°C in our study, akin to measurements in various cities like Phoenix, Singapore, Munich, Gothenburg and Melbourne (Meili et al., 2021).

UHI impact at night is evident due to absorbed solar radiation being slowly released, influencing subsequent day temperatures (Norton et al., 2015). Tree-lined streets showed significant summertime air temperature reductions of 0.5 to 2.0°C (McDonald et al., 2021). Additionally, street orientation and tree proximity to buildings affect air temperatures, aligning with our midday measurements ranging from 1.1°C to 5.3°C (Ibrahim, 2013).

Field measurements emphasized the thermal advantages of green spaces, particularly urban parks, with significant temperature differences observed, aligning with our findings regarding Skopje's City Park as the coolest area (Papangelis et al., 2012; Vidrich & Medved, 2013). This emphasizes the importance of trees in reducing daytime temperatures and extending cooling effects into the night, benefiting public health (Meili et al., 2021). Trees, either solitary or in clusters, have a considerable cooling impact by blocking solar

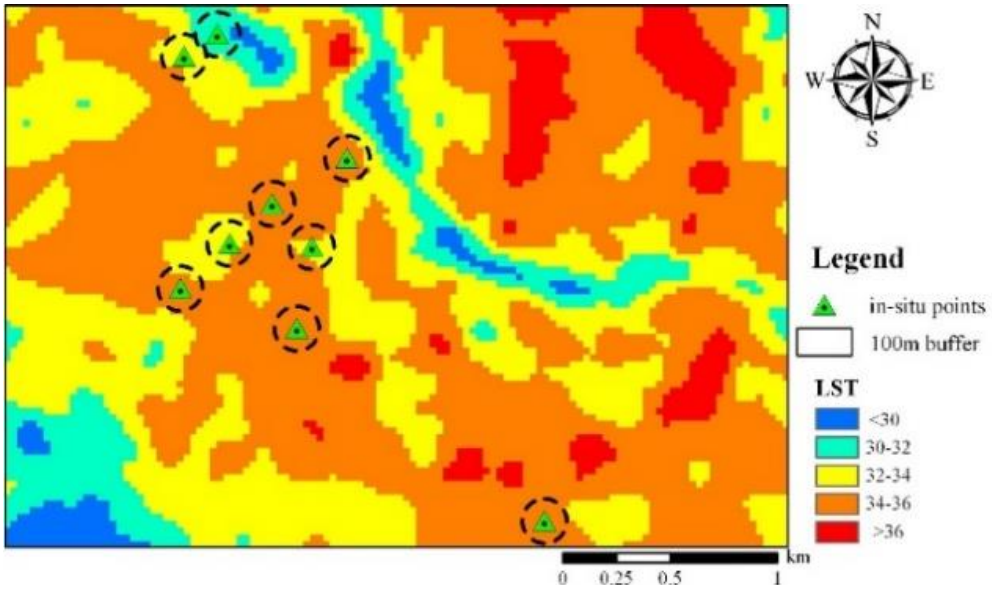

Figure 6: LST classification in 5 different classes

radiation and aiding evapotranspiration. Urban forests and tree-lined streets exhibit noticeable air temperature reductions, on average by 0.8°C under trees and up to 1.6°C within street canyons adjacent to parks (Vidrich & Medved, 2013).

It's essential to consider the interplay between vegetation and the albedo effect when analyzing their impact on urban temperature regulation. In urban areas like Sacramento, Houston, and Chicago, a rise in surface albedo was associated with a substantial decrease in daily air temperatures by 2.3°C (Jandaghian & Akbari, 2018). A study in Montreal demonstrated that enhancing albedo reduced daily air temperatures by 0.7°C, raised dew point temperatures by 0.4°C, and improved heat stress indices by 3%, collectively contributing to a nearly 4% reduction in heat-related mortality during two heat waves (Zahra & Umberto, 2019).

Earlier data suggested that modifying surface albedo alongside increasing vegetation could lower air temperatures by as much as 4°C (Taha, 199, Lopez-Cabeza et al., 2022). However, while high-albedo surfaces have the potential to decrease air temperatures, they might simultaneously heighten heat stress risk for pedestrians (Erell et al., 2014). It's crucial to advocate for active transport while ensuring conducive conditions.

In cities affected by UHI effects, extreme heat isn't evenly distributed, forming 'hot spots' due to intense urban development with limited vegetation and water, mirroring findings in Skopje similar to the Norton study. The city's General Urban Plan (2012) allocated 6% of its total area to green spaces, crucial in mitigating heat (Study on greening in the area of the City of Skopje, 2012). Research from Melbourne suggested a 10% rise in vegetation could reduce daytime urban temperatures by about 1°C (Coutts & Harris, 2013). Land cover analysis in Skopje (2013-2017) showed a slight decrease in vegetated areas alongside expanding urban zones, impacting local temperatures (Kaplan et al., 2018).

Unfortunately, in many Southern and South-Eastern European cities, including ours, the cooling effectiveness of urban trees diminishes during extreme heat periods (Schwaab et al., 2021). Anticipated dry summers in Europe will further reduce vegetation benefits (Christidis & Stott, 2021), necessitating immediate action. Green spaces play a vital role in stabilizing temperature variations caused by construction materials, contributing to 'cool islands' within cities (Andoni & Wonorahardjo, 2018). With urban expansion, more land covered by heat-retaining surfaces limits green spaces, exacerbating the UHI effect and causing outdoor thermal discomfort (Mirzaei, 2015).

In heat-wave conditions, even a 1°C rise above the heat cut-off point (30.8°C) increases mortality by 4.8% (Luber & McGeehin, 2008). Extreme heat remains a significant cause of preventable deaths globally, especially during intense heat waves, affecting various vulnerable groups, including children, older adults, and socioeconomically marginalized populations (Mayrhuber et al., 2018).

Urbanization, coupled with UHI effects and global warming, escalates thermal stress in cities, posing a growing concern for public health (Gabriel & Endlicher, 2011). Estimates suggest that the costs of heat-related health damage in Skopje reach MKD 170 million per year, far outweighing the MKD 12 million spent annually on heat-health adaptation measures (Kendrovski et al., 2014). Projections indicate a stark increase in heat-related deaths in Skopje in the coming decades compared to the baseline period of 1986-2005.

Addressing these challenges requires consistent and comprehensive health action plans tailored to regional conditions (Lancet, 2021 & Kocubovski et al., 2023). Despite recent advocacy by the World Health Organization to include health authorities in climate change mitigation efforts, healthcare facilities' preparedness remains inconsistent, posing potential challenges in treating patients during extreme heat events.

The investigation into UHIs benefits significantly from a dual approach integrating in-situ measurements and remote sensing analysis. While in-situ measurements offer precision, they are limited to specific locations and can be time-consuming. In contrast, remote sensing provides a more practical solution by capturing data across expansive regions, allowing for a comprehensive analysis of UHI patterns on a larger scale. Additionally, remote sensing provides a wealth of data beyond temperature, including estimations of crucial factors such as vegetation cover, which plays a pivotal role in mitigating UHI effects.

The synergy between these methods is evident in their distinct advantages. In-situ measurements yield precise data for specific points, while remote sensing ensures efficiency and a broader scope for analysis. Moreover, remote sensing allows researchers to delve into historical data, enabling the identification of UHI development trends over time. This historical perspective is invaluable for devising effective urban planning and management strategies.

One illustrative example is the classification depicted in Figure 6, showcasing the segmentation of the study area into five temperature classes. This visual representation not only highlights the spatial distribution of temperature variations, from cold to warm areas, but also facilitates a clearer understanding of UHI effects in different zones.

The integration of in-situ measurements and remote sensing analysis offers a comprehensive insight into the multifaceted nature of UHIs. While in-situ measurements offer precise localized data, remote sensing extends the analysis horizon, providing a comprehensive view of diverse factors influencing UHI, including historical trends and the impact of vegetation cover. This combined approach constitutes a robust toolset for both understanding and managing UHIs in urban settings.

The convergence of in-situ measurements and remote sensing analysis not only enhances our comprehension of UHIs but also offers actionable insights crucial for effective urban planning and sustainable development. By amalgamating precise local data from in-situ measurements with the broader perspective afforded by remote sensing, decision-makers can formulate targeted strategies to mitigate UHI effects.

This comprehensive approach empowers city planners and policymakers with a nuanced understanding of the complex interplay between urban landscapes and temperature variations. The insights derived aid in identifying high-risk zones prone to UHI effects, prioritizing areas for green infrastructure development, and implementing heat reduction measures where they are most impactful. Furthermore, it assists in optimizing resource allocation by directing efforts toward areas most in need of intervention.

In essence, the synergy between in-situ measurements and remote sensing not only deepens our understanding of UHIs but also equips stakeholders with the knowledge necessary to implement informed and strategic interventions for creating more resilient and sustainable urban environments.

CONCLUSION

In summary, our study highlights the significant impact of trees on the diurnal pattern of urban air temperature modification. We've observed that evapotranspiration from trees offers substantial cooling effects during both day and night, yet there's a delicate balance to strike between maximizing daytime cooling and preserving radiative cooling at night, especially concerning street trees and their geometry.

The vulnerability of urban residents to medical and economic challenges due to extreme temperatures is evident. Access to green spaces, particularly those with trees like parks and gardens, emerges as a potential solution to

mitigate thermal stress caused by the urban heat island effect during the day, safeguarding public health.

Our findings underline the urgency for strategic tree planting near streets and boulevards to combat UHI and reduce health risks for pedestrians and cyclists facing soaring midday temperatures. Further investigations are essential, encompassing additional parameters like canopy height and volume measurement, assessing the impact on human health, and considering relative humidity variations across micro-locations and times of the day. It's crucial to acknowledge the need for ongoing research to validate and extend these findings to diverse urban settings, especially amid potential urban expansion and changing climates. Our study, leveraging both in-situ and remote sensing data, contributes to the broader understanding of UHI dynamics and holds implications for sustainable urban development and environmental management.

REFERENCES

[1] Aalto, I. J., Maeda, E. E., Heiskanen, J., Aalto, E. K., & Pellikka, P. K. E. (2022). Strong influence of trees outside forest in regulating microclimate of intensively modified Afromontane landscapes. *Biogeosciences*, *19* (17), 4227-4247.

[2] AccuWeather. (2022). Skopje July Weather. AccuWeather. Retrieved from https://www.accuweather.com/en/mk/skopje/227397/july-weather/227397.

[3] Almeida, C. R. D., Teodoro, A. C., & Gonçalves, A. (2021). Study of the urban heat island (UHI) using remote sensing data/techniques: A systematic review. *Environments*, *8*(10), 105.

[4] Alonzo, M., Baker, M. E., Gao, Y., & Shandas, V. (2021). Spatial configuration and time of day impact the magnitude of urban tree canopy cooling. *Environmental Research Letters*, *16*(8), 084028.

[5] Alqasemi AS, Hereher ME, Kaplan G, Al-Quraishi AM, Saibi H. Impact of COVID-19 lockdown upon the air quality and surface urban heat island intensity over the United Arab Emirates. Science of the Total Environment. 2021 May 1;767:144330.

[6] Andoni, H., & Wonorahardjo, S. (2018, May). A review on mitigation technologies for controlling urban heat island effect in housing and settlement areas. In *IOP Conference Series: Earth and Environmental Science* (Vol. 152, No. 1, p. 012027). IOP Publishing.

[7] Avdan, U., & Jovanovska, G. (2016). Algorithm for automated mapping of land surface temperature using LANDSAT 8 satellite data. *Journal of sensors*, *2016*, 1-8.

[8] Chatterjee, U., & Majumdar, S. (2022). Impact of land use change and rapid urbanization on urban heat island in Kolkata city: A remote sensing based perspective. *Journal of Urban Management*, *11*(1), 59-71.

[9] Chen, X. L., Zhao, H. M., Li, P. X., & Yin, Z. Y. (2006). Remote sensing image-based analysis of the relationship between urban heat island and land use/cover changes. *Remote sensing of environment*, *104*(2), 133-146.

[10] Chen, X., Zhou, Z., Teng, M., Wang, P., & Zhou, L. (2015). Accumulation of three different sizes of particulate matter on plant leaf surfaces: effect on leaf traits. *Archives of Biological Sciences*, *67*(4), 1257-1267.

[11] Christidis, N., & Stott, P. A. (2021). The influence of anthropogenic climate change on wet and dry summers in Europe. *Science Bulletin*, *66*(8), 813-823.

[12] Coutts, A. M., Beringer, J., & Tapper, N. J. (2007). Impact of increasing urban density on local climate: Spatial and temporal variations in the surface energy balance in Melbourne, Australia. *Journal of Applied Meteorology and Climatology*, *46*(4), 477-493.

[13] Coutts, A., & Harris, R. (2013). A multi-scale assessment of urban heating in Melbourne during an extreme heat event.

[14] Despini, F., Ferrari, C., Santunione, G., Tommasone, S., Muscio, A., & Teggi, S. (2021). Urban surfaces analysis with remote sensing data for the evaluation of UHI mitigation scenarios. *Urban Climate*, *35*, 100761.

[15] Donevska, K., & Panov, A. (2019). Climate change impact on water supply demands: case study of the city of Skopje. *Water Supply*, *19*(7), 2172-2178.

[16] Elmqvist, T., Setälä, H., Handel, S. N., van der Ploeg, S., Aronson, J., Blignaut, J. N., & de Groot, R. (2015). Benefits of restoring ecosystem services in urban areas. *Current opinion in environmental sustainability*, *14*, 101-108.

[17] Erell, E., Pearlmutter, D., Boneh, D., & Kutiel, P. B. (2014). Effect of high-albedo materials on pedestrian heat stress in urban street canyons. *Urban climate*, *10*, 367-386.

[18] Fuladlu, K. (2022). Thermal Response to Land-Use Land-Cover Patterns: An Experimental Study in Famagusta, Cyprus. *CLEAN–Soil, Air, Water*, *50*(9), 2100284.

[19] Fuladlu, K., & Altan, H. (2021). Examining land surface temperature and relations with the major air pollutants: A remote sensing research in case of Tehran. *Urban Climate*, *39*, 100958.

[20] Gabriel, K. M., & Endlicher, W. R. (2011). Urban and rural mortality rates during heat waves in Berlin and Brandenburg, Germany. *Environmental pollution*, *159*(8-9), 2044-2050.

[21] Hondula, D. M., & Barnett, A. G. (2014). Heat-related morbidity in Brisbane, Australia: spatial variation and area-level predictors. *Environmental health perspectives*, *122*(8), 831-836.

[22] Huang, Z., Wu, C., Teng, M., & Lin, Y. (2020). Impacts of tree canopy cover on microclimate and human thermal comfort in a shallow street canyon in Wuhan, China. *Atmosphere*, *11*(6), 588.

[23] Ibrahim, H. (2013). A new paradigm of urban development: Envisioning sustainable futures in Qatar. *Sustainable Development and Planning, WIT Transactions on Ecology and The Environment*, *173*, 299-310.

[24] Jandaghian, Z., & Akbari, H. (2018). The effect of increasing surface albedo on urban climate and air quality: A detailed study for Sacramento, Houston, and Chicago. *Climate*, *6*(2), 19.

[25] Jiao, M., Zhou, W., Zheng, Z., Wang, J., & Qian, Y. (2017). Patch size of trees affects its cooling effectiveness: A perspective from shading and transpiration processes. *Agricultural and Forest Meteorology*, *247*, 293-299.

[26] Jim, C. Y. (2019). Soil volume restrictions and urban soil design for trees in confined planting sites. *Journal of Landscape Architecture*, *14*(1), 84-91.

[27] Kaplan G, Avdan U, Avdan ZY. Urban heat island analysis using the landsat 8 satellite data: A case study in Skopje, Macedonia. InProceedings 2018 Mar 22; 2(7): 358.

[28] Kaplan, G. (2019). Evaluating the roles of green and built-up areas in reducing a surface urban heat island using remote sensing data. *Urbani izziv*, *30*(2), 105-112.

[29] Kendrovski, V. T. (2006). The impact of ambient temperature on mortality among the urban population in Skopje, Macedonia during the period 1996–2000. *BMC Public Health*, *6*(1), 1-6.

[30] Kendrovski, V., Spasenovska, M., & Menne, B. (2014). The public health impacts of climate change in the former Yugoslav Republic of Macedonia. *International Journal of Environmental Research and Public Health*, *11*(6), 5975-5988.

[31] Kocubovski, M., Ristovska, G., Petrova, A., Bukovetz, J., Disho, K., Tosev, T. H., & Petreski, A. (2023). Review of policies and actions on tackling global climate change-COP26-is this the last chance?. *Archives of Public Health*, *15*(1).

[32] Lancet, T. (2021). Health in a world of extreme heat. *Lancet (London, England)*, *398*(10301), 641.

[33] Li, J. J., Wang, X. R., Wang, X. J., Ma, W. C., & Zhang, H. (2009). Remote sensing evaluation of urban heat island and its spatial pattern of the Shanghai metropolitan area, China. *Ecological Complexity*, *6*(4), 413-420.

[34] Lopez-Cabeza, V. P., Alzate-Gaviria, S., Diz-Mellado, E., Rivera-Gomez, C., & Galan-Marin, C. (2022). Albedo influence on the microclimate and thermal comfort of courtyards under Mediterranean hot summer climate conditions. *Sustainable Cities and Society*, *81*, 103872.

[35] Luber, G., & McGeehin, M. (2008). Climate change and extreme heat events. *American journal of preventive medicine*, *35*(5), 429-435.

[36] Mayrhuber, E. A. S., Dückers, M. L., Wallner, P., Arnberger, A., Allex, B., Wiesböck, L., Wanka, A., Kolland, F., Eder, R., Hutter, H.P., & Kutalek, R. (2018). Vulnerability to heatwaves and implications for public health interventions–A scoping review. *Environmental Research*, *166*, 42-54.

[37] McDonald, R. I., Biswas, T., Sachar, C., Housman, I., Boucher, T. M., Balk, D., Nowak, D., Spotswood, E., Stanley, C.K., & Leyk, S. (2021). The tree cover and temperature disparity in US urbanized areas: Quantifying the association with income across 5,723 communities. *PloS one*, *16*(4), e0249715.

[38] McPherson, E. G., Xiao, Q., van Doorn, N. S., Johnson, N., Albers, S., & Peper, P. J. (2018). Shade factors for 149 taxa of in-leaf urban trees in the USA. *Urban Forestry & Urban Greening*, *31*, 204-211.

[39] Meili, N., Manoli, G., Burlando, P., Carmeliet, J., Chow, W. T., Coutts, A. M., Roth, M., Velasco, E., Vivoni, E.R., & Fatichi, S. (2021). Tree effects on urban microclimate: Diurnal, seasonal, and climatic temperature differences explained by separating radiation, evapotranspiration, and roughness effects. *Urban Forestry & Urban Greening*, *58*, 126970.

[40] Meineke, E., Youngsteadt, E., Dunn, R. R., & Frank, S. D. (2016). Urban warming reduces aboveground carbon storage. *Proceedings of the Royal Society B: Biological Sciences*, *283*(1840), 20161574.

[41] Mirzaei, P. A. (2015). Recent challenges in modeling of urban heat island. *Sustainable cities and society*, *19*, 200-206.

[42] Ngie, A., Abutaleb, K., Ahmed, F., Darwish, A., & Ahmed, M. (2014). Assessment of urban heat island using satellite remotely sensed imagery: a review. *South African Geographical Journal= Suid-Afrikaanse Geografiese Tydskrif*, *96*(2), 198-214.

[43] Norton, B. A., Coutts, A. M., Livesley, S. J., Harris, R. J., Hunter, A. M., & Williams, N. S. (2015). Planning for cooler cities: A framework to prioritise green infrastructure to mitigate high temperatures in urban landscapes. *Landscape and urban planning*, *134*, 127-138.

[44] Oke, T. R. (1988). The urban energy balance. *Progress in Physical geography*, *12*(4), 471-508.

[45] Papangelis, G., Tombrou, M., Dandou, A., & Kontos, T. (2012). An urban “green planning” approach utilizing the Weather Research and

Forecasting (WRF) modeling system. A case study of Athens, Greece. *Landscape and urban planning*, *105*(1-2), 174-183.

[46] Rahman, M. A., Armson, D., & Ennos, A. R. (2015). A comparison of the growth and cooling effectiveness of five commonly planted urban tree species. *Urban Ecosystems*, *18*, 371-389.

[47] Rahman, M. A., Moser, A., Rötzer, T., & Pauleit, S. (2017). Within canopy temperature differences and cooling ability of Tilia cordata trees grown in urban conditions. *Building and Environment*, *114*, 118-128.

[48] Ren, Z., Zhao, H., Fu, Y., Xiao, L., & Dong, Y. (2022). Effects of urban street trees on human thermal comfort and physiological indices: a case study in Changchun city, China. *Journal of Forestry Research*, *33*(3), 911-922.

[49] Rulebook for Urban Planning. Official Journal of the Republic of Macedonia No. 225/2020.

[50] Schwaab, J., Meier, R., Mussetti, G., Seneviratne, S., Bürgi, C., & Davin, E. L. (2021). The role of urban trees in reducing land surface temperatures in European cities. *Nature communications*, *12*(1), 6763.

[51] Smithers, R. J., Doick, K. J., Burton, A., Sibille, R., Steinbach, D., Harris, R., ... & Blicharska, M. (2018). Comparing the relative abilities of tree species to cool the urban environment. *Urban Ecosystems*, *21*, 851-862.

[52] Sperry, J. S., Venturas, M. D., Todd, H. N., Trugman, A. T., Anderegg, W. R., Wang, Y., & Tai, X. (2019). The impact of rising CO2 and acclimation on the response of US forests to global warming. *Proceedings of the National Academy of Sciences*, *116*(51), 25734-25744.

[53] Steensen, B. M., Marelle, L., Hodnebrog, Ø., & Myhre, G. (2022). Future urban heat island influence on precipitation. *Climate Dynamics*, *58*(11-12), 3393-3403.

[54] Study on greening in the area of the City of Skopje, DEKONS EMA DOO Skopje; 2012.

[55] Taha, H. (1997). Urban climates and heat islands: albedo, evapotranspiration, and anthropogenic heat. *Energy and buildings*, *25*(2), 99-103.

[56] Taha, H. (1997). Urban climates and heat islands: albedo, evapotranspiration, and anthropogenic heat. *Energy and buildings*, *25*(2), 99-103.

[57] Tao, L., Ryu, D., Western, A., & Boyd, D. (2020). A new drought index for soil moisture monitoring based on MPDI-NDVI trapezoid space using MODIS data. *Remote Sensing*, *13*(1), 122.

[58] Tomlinson, C. J., Chapman, L., Thornes, J. E., & Baker, C. (2011). Remote sensing land surface temperature for meteorology and climatology: A review. *Meteorological Applications*, *18*(3), 296-306.

[59] Turner-Skoff, J. B., & Cavender, N. (2019). The benefits of trees for livable and sustainable communities. *Plants, People, Planet*, *1*(4), 323-335.

[60] Vailshery, L. S., Jaganmohan, M., & Nagendra, H. (2013). Effect of street trees on microclimate and air pollution in a tropical city. *Urban forestry & urban greening*, *12*(3), 408-415.

[61] Taha, H., Akbari, H., & Rosenfeld, A. (1991). Heat island and oasis effects of vegetative canopies: micro-meteorological field-measurements. *Theoretical and Applied Climatology*, *44*, 123-138.

[62] *WHO Heat-Health Action Plan to prevent consequences on the health of the population in the Republic of Macedonia*, Skopje; 2011.

[63] Wang, Y., & Akbari, H. (2016). The effects of street tree planting on Urban Heat Island mitigation in Montreal. *Sustainable cities and society*, *27*, 122-128.

[64] Wang, C., Wang, Z. H., & Yang, J. (2018). Cooling effect of urban trees on the built environment of contiguous United States. *Earth's Future*, *6*(8), 1066-1081.

[65] Yue, W., Xu, J., Tan, W., & Xu, L. (2007). The relationship between land surface temperature and NDVI with remote sensing: application to Shanghai Landsat 7 ETM+ data. *International journal of remote sensing*, *28*(15), 3205-3226.

[66] Zahra, J., & Umberto, B. (2019, September). Effects of increasing urban albedo in the Greater Toronto Area. In *IOP Conference Series: Materials Science and Engineering* (Vol. 609, No. 7, p. 072002). IOP Publishing.

[67] Ziter, C. D., Pedersen, E. J., Kucharik, C. J., & Turner, M. G. (2019). Scale-dependent interactions between tree canopy cover and impervious surfaces reduce daytime urban heat during summer. *Proceedings of the National Academy of Sciences*, *116*(15), 7575-7580.

Vesna Grujoska
MSc in Civil Engineering
Ss. Cyril and Methodius University in Skopje
Faculty of Civil Engineering
N. Macedonia
vesnagrujoska@yahoo.com

Todorka Samardzioska
PhD, Full Professor
Ss. Cyril and Methodius University in Skopje
Faculty of Civil Engineering
N. Macedonia

STATE-OF-THE-ART OF BACTERIA-BASED SELF-HEALING CONCRETE

Crack appearance in the concrete structure due to the low tensile strength is inevitable and can cause degradation of the structure integrity. Bacteria addition in the concrete structure is one promising way of achieving crack healing. When bacteria concrete is used, the bacteria can be added directly in the mixture or protected in different types of materials, usually lightweight materials. Along with the bacteria, additionally nutrients and calcium source are part of the mixture, as well. As a result, calcium carbonate is precipitated in the vicinity of the crack which will fill the crack and block all the harmful substances to penetrate in the concrete structure.

Over the years, many papers are witnessing the successful work of bacteria based self–healing concrete where the maximum crack width healed can reach almost 1 mm (0.97 mm).

However, it is worth mentioning that the addition of bacteria to the concrete mixture certainly causes some complications in the preparation process and this material should be observed at a completely new level.

Based on available experimental work, a review from the perspective of encapsulation material, incubation conditions, strength, sustainability and some closely related properties are discussed.

Keywords: concrete, bacteria, self-healing, encapsulation

1. INTRODUCTION

Concrete is currently most used material globally due to the fact that is relatively cheap and available. The speed of urbanization is faster than ever and more intensive than ever. According to Justo-Reinoso et all.[6] this era might be remembered as “concrete era” for future generations. Bagga et all [2] are predicting that every month, in the next 40 years, a city big as New York will be build.

Appearances of cracks due to the low tensile strength are considered the biggest drawback of concrete. Smaller crack widths that are 0.2-0.3 mm are not considered harmful and dangerous for the integrity of the concrete

structure but are allowing the harmful substances to get in the concrete structure and cause deterioration and steel corrosion, which can further lead to serious structure damage. Thereby, monitoring and control of the concrete structures must be mandatory. On the other hand, costs for maintenance are high. In Great Britain, the costs for maintenance are almost half (44.6%) of the total budget assigned for infrastructure [15]. Therefore, a compromise in between must be provided.

Self-healing concrete is created material as a reaction to the high maintenance costs and it is inspired by the ability of the human body to self-heal after injury.

Addition of bacteria into the concrete structure is just one way of achieving self-healing but is considered a successful way according to the results obtained from different experimental work. It is still considered as a material in development phase and that is why a lot of variation in the laboratory work can be observed.

2. STATE-OF-THE-ART

The concept of self-healing is known concept years back as further hydrations of unhydrated cement that can fill small cracks. Nevertheless, this way of self-healing is just a result of use the standard components of the concrete mixture. Today, the progress in the field of self-healing concrete is remarkable. The novelty in self-healing comes when additional materials are incorporated in the concrete structure in order to get planned crack filling.

Many different materials are tested as potential healing agents.

Van Tittelboom et al. [17] in their review paper presented the evolution of the published paper through the years, pointing up the publication of White et al. in 2001 as an impulse in the research area of self-healing materials.

In the last few decades, the intensity of research in the field of bacteria concrete can be noticed. The beginnings of the self-healing bacteria concrete are linked to the initial research of professor Jonkers [5]. They investigated self-healing concrete with metabolic mineral production by directly adding the bacteria Bacillus cohnii and calcium lactate to the concrete mix.

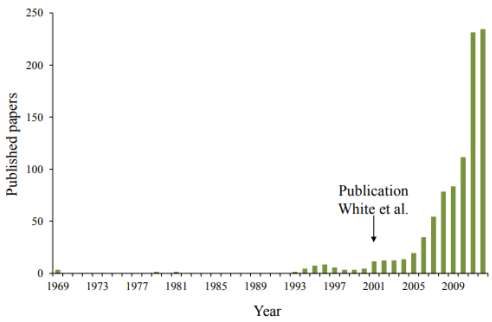

Figure 1. Scientific achievements in the area of self-healing materials through the years [17]

Particles with a size of 1-5 μm appeared on the surface of the crack on the control samples at the age of 7 and 28 days. In contrast to the control samples, in the samples that contained bacteria and calcium lactate, the size of the mineral particles that appeared were 20-80 μm, but only in the 7 days old samples. At the age of 28 days, this influence was unnoticeable. This is a consequence of the fact that survival rate of the bacteria when added unprotected in the concrete mixture is poor. As a solution to the short lifespan of the bacteria, protection is required by encapsulating the self-healing agent in protective material. In the Table 1 are presented some of the materials that are usually used as a protection material for bacteria.

Wiktor et al. [22] tested encapsulation process with the use of expanded clay. Oxygen consumption test and crack closure test after 100 days showed viability of bacteria and complete closure of 0.46 mm crack width, when samples healed full immersed in water.

Tziviloglou et al. [16] tested different healing regimes for samples healing (fully immersion in water and wet/dry cycles). Wet/dry cycles are simulating more realistic exploitation conditions for the construction. The results after 28 and 56 days fully immersion showed that regained water tightness (RWT) was 31 and 82% for Control samples, and for Bacteria samples 69% and 91% RWT after 28 and 56 days, respectively. Control samples exposed on wet/dry cycles showed very poor results to the crack closure, but bacterial samples showed 98% crack closure after 56 days of curing.

Tan et al. [9] tested different duration of wet/dry cycle (3 days wet/4 days dry). Longer exposure on air without water negatively affected the process of self–healing.

Table 1. Different type of encapsulation material, calcium source and growth media

Encapsulation material	Reference	Type of bacteria and growth media
Microencapsulation	Paine et al. [9]	Bacillus pseudofirmus Calcium acetate, yeast extract, glucose
	Wang et al. [19]	Bacillus sphaericus, Calcium nitrate, yeast extract, urea
Aerated concrete granules (ACG)	Tan et al. [14]	Bacillus cohnii, Calcium nitrate, yeast extract
Expanded perlite	Alazharie et al. [1]	Bacillus pseudofirmus Calcium acetate, yeast extract
	Paine et al. [8]	Bacillus pseudofirmus Calcium acetate, yeast extract
Expanded clay	Wiktor et al. [22]	Bacillus alkalinitrilicus, Calcium lactate, yeast extract
	Tziviloglou et al. [16]	Bacillus cohnii, Calcium lactate, yeast extract
	Risdanareni et al. [13]	Bacillus sphaericus, Calcium nitrate, Yeast extract

Generated material in the cracks is usually calcium carbonate. Bacteria can precipitate calcium carbonate through few pathways, but usually the following is required:

(1) sufficient concentration of dissolved inorganic carbon in the pore water in the vicinity of crack to enable formation of CO_3^{2-} ions,
(2) local pH change
(3) attraction of Ca^{2+} ions to the negatively charge bacteria surface, where bacteria may act as a nucleation point, and
(4) sufficient quantity of Ca^{2+} ions to precipitate calcium carbonate, Tan et al [14].
Microbially induced calcium precipitation (MICP) can be achieved through three pathways [1]:

- enzymatic hydrolysis of urea
- dissimilation of nitrates and
- aerobic metabolic conversion of calcium salts.

Urea hydrolysis is an effective way of calcite precipitation with ureolytic bacteria. Wang et al. [21] emphasised that due to the high $CaCO_3$ precipitation, hydrolysis of urea is most commonly used.

The minimum number of spores required for the self-healing process to occur was considered for the first time in the paper of Alazhari et al. [1]. Expanded perlite as 20% replacement of aggregate with 8 x 10^9 spores/g calcium acetate can provide self-healing of cracks.

Wang et al [18] used diatomaceous earth (DE) as protective carrier for bacteria. DE was considered as a successful carrier for bacteria due to the high absorption capacity. Cracks with width 0.15-0.17 mm were partially of fully closed depending on the immersion media.

Activation of the bacteria at the same moment of crack formation is important parameter for the self-healing process to occur. In order to prevented earlier activation of bacteria, separately encapsulation of bacteria and nutrients was considered by Paine et al. [10] Expanded perlite as encapsulation material was coated with dual layer of sodium silicate and Portland fly ash cement to prevent leakage of the encapsulated material.

Ceramsite as bacteria carrier was investigated by Chen et al. [4]. Separately were encapsulated bacteria and nutrients (yeast extract and sucrose). Four different mixtures were prepared, all of them with ceramsite: C1- without any addition, C2 – just glucose added, C3- Bacillus Mucilaginous and Brewers Yeast and C4 bacteria and nutrients. Test results of water permeability showed initial water permeability coefficient 7.9~8.3 x 10^{-5} m/s.

After 21 days of healing, water permeability coefficient dropped to $5.3x10^{-6}$ ~ 9.5×10^{-6} m/s for C1, C2 and C3, and for C4 the value reached 0.8×10^{-7} m/s.

Graphite nanoplateletes (GNP) compared to Light weight aggregate (LWA) were investigated by Khaliq et al [7]. Specimens were pre-cracked on 3, 7, 14 and 28 days and also observed during the 28 days healing period (3, 7 ,14 and 28 days). Results showed that specimens pre-cracked at early age of 3 and 7 days showed maximum healing efficiency when bacteria was incorporated in GNP, but at later age pre-cracked specimens with LWA incorporated bacteria showed better results. This can be explained with the fact that the process of continuous hydration make denser structure that can destroy the GNP.

Natural fiber as bacteria protection with three different type of bacteria Bacillus subtilis, Bacillus cohnii and Bacillus sphaericus were tested by Rauf et al [12] Jute, flax and coir fiber were used and among them, flax fiber showed results as the best host environment for bacteria considering the healing ability. Flax and jute fiber in combination with Bacillus sphearicus showed 95.1% and 98.4% regained compressive strength. Average surface healing on fiber concrete was 75-85% and 60-65% at 7 and 28 days pre-cracked specimens, respectively.

Wang et al. [20] used silica gel and polyurethane (PU) for bacteria immobilization. Despite the fact that the amount of precipitation material in the case of silica gel immobilization bacteria was higher compared to the polyurethane immobilized bacteria, the regained strength of samples with polyurethane showed higher values but the main reason might be the PU itself. As for the self-healing efficiency testes through water permeability test, PU immobilized bacteria showed lower values of water permeability coefficient.

Wang et al. [19] considered microencapsulation as a way of protection of bacteria. They observed maximum crack width healed in bacteria specimens of 0.97mm.

Self-healing concrete is elevating the regular concrete level in terms of sustainability by eliminating the repairing phase. However, the contribution can be even greater when using some waste materials.

Recycled concrete aggregates is good substitute material for the natural aggregate usually used in the concrete mixture. Despite the fact that natural aggregate has better characteristics, as a natural material, the resources are limited. As a carrier for bacteria and when used in reasonable amount, recycled concrete aggregate from old demolished concrete structures was considered good substitute material, showing bacteria concrete crack closure of 0.6 mm, after 28 days of healing [21].

Xu et al. [23] used rubber particle (waste rubber) as bacteria carrier. Using waste materials as a carrier for bacteria is beneficial for the environment and supports nowadays struggle of gaining sustainable materials. Two different mixtures were prepared with different size of particles, 1-3 mm (SRC-L) and 0.2-0.4mm (SRC-S). Interesting results were observed from this paper that crack width of 0.86 mm was completely healed and crack width of 0.38 mm was only 11% healed (SRC-L). This is indication that bacteria is not uniformly distributed in the concrete mixture. Also healing of specimens containing larger rubber particles SRC-L) were showing better crack closure results compared with specimens containing smaller rubber particles (SRC –S). 50% of the cracks with initial width of 0.22 – 0.86 mm were 100% healed (in SRC-L specimens) compared to only few cracks with initial width 0.22-0.54mm healed 100% (in SRC-S). This may be because bacteria have more space to grow.

Chahal et al [3] considered replacement of cement with fly ash. Cement replacement with 10, 20 and 30 % fly ash was combined with three different bacteria concentrations 10^3, 10^5, 10^7 cells/ml. After 28 days, bacteria fly ash concrete showed increase of compressive strength of 22%.

Bacteria is not only contributing to the self-healing process, but is playing an important role in the strength properties as well. Ramachandran et al [11] were among the first who investigated the influence of bacteria on the concrete strength by adding live and autoclaved bacteria. When using Bacillus pasteurii bacteria with concentration of 7.8 x 10^3 cells/m^3, 18% compressive strength improvement was noticed. Except live bacteria, autoclaved bacteria also showed improvement in the concrete strength properties, playing a roll of fibers.

Bacteria based self-healing concrete can consider many more aspects that are affecting the process (nutrients and calcium source effect, different temperature exposure,

optimization of the process, a life cycle assessment perspective and many more). That is why this material is so long stuck in the development phase. Laboratory work are best way for testing new materials but also expensive and last long. Data modeling can be consider as a step forward in this area.

3. CONCLUSION

Bacteria-based self-healing concrete is a promising solution for maintenance of the concrete structures. Results of the experimental work, so far, are showing that micro-cracks can repair themselves and penetration of harmful substances can be prevented if proper materials are added in the concrete mixture. Bacteria-based self-healing concrete is getting huge attention due to the successful results of healing cracks up to 0.97mm. It is important to mention that with the addition of bacteria, the concrete mixture becomes more complex to work with. Directly added bacteria in the mixture cannot survive for a long period, so encapsulation of bacteria can be considered as a solution. Different encapsulation material can be part of the mixture but they are usually lightweight materials that affect the strength properties. Therefore, the quantity of these materials should be limited. Furthermore, using waste materials can contribute to the concept of sustainability of self-healing materials.

REFERENCES

[1] Alazhari M., Sharma T., Heath A., Cooper R., Paine K. (2018), “Application of expanded perlite encapsulated bacteria and growth media for self-healing concrete”, Constr Build Material; 160:610–9.

[2] Bagga M., Hamley-Bennett C., Alex A., Freeman B L., Justo-Reinoso I, Mihai I C., Gebhard S., Paine K, Jefferson A D., Masoero E., Ofiţeru D I. (2022), “Advancements in bacteria based self-healing concrete and the promise of modelling“, Construction and Building Materials, Volume 358, 129412, ISSN 0950-0618, https://doi.org/10.1016/j.conbuildmat.2022.129412.

[3] Chahal N., Siddique R., Rajor A. (2012), “Influence of bacteria on the compressive strength, water absorption and rapid chloride permeability of fly ash concrete“, Constr Build Mater 28:351–6.

[4] Chen H., Qian C., Huang H. (2016): “Self-healing cementitious materials based on bacteria and nutrients immobilized respectively“, Constr Build Mater 2016; 126:297–303.

[5] Jonkers H M, Thijssen A, Muyzer G, Copuroglu O, Schlangen E (2010), “Application of bacteria as self- healing agent for the development of sustainable concrete“, Ecol Eng 36: 230–235.

[6] Justo- Reinoso I., Heath A., Gebhard S., Paine K. (2021), “Aerobic non-ureolytic bacteria-based self-healing cementitious composites: A comprehensive review”, Journal of Building Engineering, Volume 42, 2021, 102834, ISSN 2352-7102.

[7] Khaliq W., Ehsan M.B. (2016), “Crack healing in concrete using various bio influenced self-healing techniques‖“, Constr Build Mater; 102:349–57.

[8] Paine K., Alazhari M., Sharma T., Cooper R., Heath A. (2016), “Design and performance of bacteria-based self-healing concrete”, in the 9th International Concrete Conference, Environment, Efficiency and Economic Challenges for, Concrete 2016, 545–554.

[9] Paine K., Horne I., Tan L., Sharma T., Heath A., Cooper R. et al. (2018), “Microencapsulated spores and growth media for self-healing mortars”. Life-Cycle Anal Assess Civ Eng Towar an Integr Vis - Proc 6th Int Symp Life-Cycle Civ Eng IALCCE 2018 2019:2247–53.

[10] Paine K., Alazhari M., Sharma T., Cooper R., Heath A. (2016), “Design and performance of bacteria-based self-healing concrete”, in the 9th International Concrete Conference, Environment, Efficiency and Economic Challenges for Concrete.

[11] Ramachandran S.K., Ramakrishnan V., Bang S.S. (2001), “Remediation of Concrete Using Microorganisms”. ACI Materials Journal. 98. 3-9. 10.14359/10154.

[12] Rauf M., Khaliq W., Khushnood R.A., Ahmed I. (2020), Comparative performance of different bacteria immobilized in natural fibers for self-healing in concrete, Construction and Building Materials, Volume 258, 2020, 119578, ISSN 0950-0618.

[13] Risdanareni P., Ma L., Wang J., De Belie N. (2022), “Suitable yeast extract concentration for the production of self-healing mortar with expanded clay as bacterial carrier“, Materiales De Construcción, 72(348), e296. https://doi.org/10.3989/mc.2022.02422.

[14] Tan L., Reeksting B., Ferrandiz-Mas V., Heath A., Gebhard S., Paine K. (2020), “Effect of carbonation on bacteria-based self-healing of cementitious composites”. Constr Build Mater 2020;257:119501 ISSN 0950-0618,https://doi.org/10.1016/j.conbuildmat.2022.127581.

[15] Tan L., Reeksting B., Justo-Reinoso I., Ferrándiz-Mas V., Heath A., Gebhard S., Paine, K. (2023), “The effect of oxygen and water on the provision of crack closure in bacteria-based self-healing cementitious

composites“ Cement and Concrete Composites.142.105201. 10.1016/j.cemconcomp.2023.105201.

[16] Tziviloglou E., Wiktor V., Jonkers H.M., Schlangen E. (2016), “Bacteria-based self-healing concrete to increase liquid tightness of cracks”. Constr. Build. Mater. 2016, 122, 118–125.

[17] Van Tittelboom K., De Belie N. (2013), “Self-healing in cementitious materials - A review”. Materials, vol. 6, 2182–2217.

[18] Wang J.Y., De Belie N., Verstraete W. (2012), “Diatomaceous earth as a protective vehicle for bacteria applied for self-healing concrete”. J Ind Microbiol Biotechnol 2012; 39:567–77.

[19] Wang J.Y., Soens H., Verstraete W., De Belie N. (2014), “Self-healing concrete by use of microencapsulated bacterial spores”. Cem Concr Res 2014; 56:139–52. 545–554.

[20] Wang J., Van Tittelboom K., De Belie N., Verstraete W. (2012), “Use of silica gel or polyurethane immobilized bacteria for self-healing concrete“, January, Construction and Building Materials 26(1):532–540.

[21] Wang X., Xu J., Wang Z., Yao W., (2022), “Use of recycled concrete aggregates as carriers for self-healing of concrete cracks by bacteria with high urease activity“, Construction and Building Materials, Volume 337, 2022,127581.

[22] Wiktor V., Jonkers H.M. (2011): “Quantification of crack-healing in novel bacteria-based self-healing concrete”. Cem. Concr. Compos. 2011, 33, 763–770.

[23] Xu H., Lian J., Gao M., Fu D., Yan Y. (2019), “Self-Healing Concrete Using Rubber Particles to Immobilize Bacterial Spores“, Materials (Basel). Jul 19;12(14):2313. doi: 10.3390/ma12142313. PMID: 31331051; PMCID: PMC6678105.

Denis Popovski
PhD, Associate Professor
Ss. Cyril and Methodius University in Skopje
Faculty of Civil Engineering
N. Macedonia
popovski@gf.ukim.edu.mk

Mile Partikov
PhD, Assistant Professor
Ss. Cyril and Methodius University in Skopje
Faculty of Civil Engineering
N. Macedonia

Ditar Memedi
MSc in Civil Engineering
Ss. Cyril and Methodius University in Skopje
Faculty of Civil Engineering
N. Macedonia

ANALYSIS OF LATERAL DEFLECTION OF STEEL MOMENT RESISTING FRAME

Steel Moment Frames, to meet certain lateral stability criteria, can often be considered overdesigned [1]. In this paper, an assessment of the behavior of steel frames under the influence of dynamic loads is made. By applying the criteria for capacitive design, proposed by Eurocode 8, the dimensioning of a 2D regular Moment Frame was carried out.

Special emphasis is placed on the implementation and interpretation of the rationality of the interstory drift sensitivity coefficient θ. To assess the rationality of the coefficient θ, a non-linear static analysis of the 2D Moment Frame was performed. In the analysis, the geometric and material nonlinearities of the elements are included using the concept of distributed plasticity. The stiffness of the beam-column connection is modeled as ideally rigid and its behavior is taken into account in the analysis. The results obtained in this way are compared with the criteria proposed by Eurocode 8.

Keywords: Steel Moment Frames, interstory drift sensitivity coefficient θ, nonlinear static analysis

1. INTRODUCTION AND MAIN CONCEPTS

Steel frames are sensitive to lateral deflections and these effects have quite an impact in the distribution of horizontal displacements and internal forces. The stresses resulting from these influences further increase the influences obtained from linear elastic analysis. The second order effects, which are obtained from these additional lateral displacements, during linear seismic analysis are taken through the sensitivity coefficient of relative storey displacements i.e θ−coefficient. This coefficient, according to the current regulation of Eurocode 8, is determined based on the expression [3]:

$$\theta_i = \frac{P_{tot,i} \cdot d_r}{V_{tot,i} \cdot h_i} \qquad (1)$$

According to Eurocode 8 [3], second-order effects should not be taken into account for frames where θ ≤ 0.1, while for θ ∈ [0.1-0.2], P-

Δ effects should be taken into account by amplifying the effects according to the expression [2]:

$$\alpha = \frac{1}{1-\theta} \tag{2}$$

2. INTERPRETATION AND THE RATIONALITY OF THE CRITERION FOR THE COEFFICIENT Θ

If a linear elastic behavior of the structure is assumed until failure, then the coefficient θ can be represented in the following form:

$$\theta_i = \frac{P_{tot,i} \cdot d_e}{V_{tot,i} \cdot h_i} \tag{3}$$

The criterion from equation (1) applied to expression (3) means that the moment generated by gravity loads ($P_{tot,i}$) in the i-th floor is less than 10% of the elastic moment load generated by the lateral stiffness of the structure [7]. Lateral stiffness is determined by the following expression:

$$k_j = \frac{V_{tot,i}}{d_e} \tag{4}$$

The above statement, n algebraic form, can be represented by the following equation:

$$\begin{aligned} \theta_i^{el} &= \frac{P_{tot,i} \cdot d_e}{V_{tot,i} \cdot h_i} \\ &= \frac{P_{tot,i}}{h_i} \cdot \left(\frac{d_e}{V_{tot,i}}\right) \\ &= \left(\frac{P_{tot,i}}{h_i} \cdot \frac{1}{k_j}\right) \leq 0.1 \end{aligned} \tag{5}$$

The criterion proposed by Eurocode 8 uses the secant lateral stiffness, i.e. expression (4) should be reduced by an appropriate q-factor, i.e.:

$$k_j = \frac{V_{tot,i}}{\boldsymbol{q} d_e} \tag{6}$$

However, the limit for the sensitivity coefficient (θ) remains at 0.1. Parallel with the coefficient Θ_i, to determine the elastic instability of the structure from vertical loads, Eurocode 3 proposes the following delimitation [2]:

$$\alpha'_{cr} = \frac{1}{\alpha_{cr}} \leq 0.1 \ \ (\alpha_{cr} = \frac{F_{cr}}{F_{Ed}} \geq 1) \tag{7}$$

The coefficient α'_{cr} for linear static analysis (Eurocode 3), corresponds to the coefficient θ_i proposed by Eurocode 8. For example, if a construction with a behavior factor q = 5 is considered, the same condition considered in an elastic area (under the influence of seismic loads) would implied θ_i^{el} = 0.1/5 = 0.02. From the last one, one can clearly notice the conservatism of this approach.

3. LINEAR STATIC ANALYSIS ACCORDING TO EUROCODE

The frame presented in Figure 1 is analyzed. The span between the columns is equal to 8m. The height of each level is 3m. For beams and columns, steel of grade S235 with $\gamma_{ov} = 1.25$ is assumed, as suggested by Eurocode 8. The cross-section of all beams is assumed to be IPE400, while for intermediate columns, HEA340 cross section is assumed. The peripheral columns are selected with a cross-section of HEA280. The intensity of constant loads and variable loads for each level is given in Figure 1.

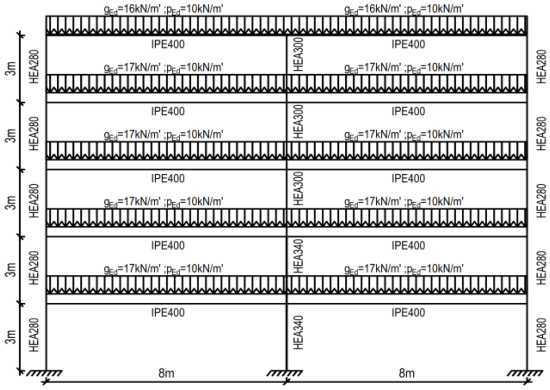

Figure 1. Analysed steel moment frame.

Due to the regularity of the frame in height, in this paper the method of equivalent lateral horizontal force was used for the linear elastic analysis.

3.1 STRONG COULMNS/WEAK BEAMS CRITERION

In order to avoid the formation of a mechanism at the local level in the columns (the so-called soft story/flexible floor), that is, to achieve a global ultimate mechanism of the structure, according to the recommendations of Eurcode 8, it is necessary to fulfill the following criteria [3]:

$$\sum W_{pl,c} > 1.3 \sum W_{pl,b} \tag{8}$$

$$2\sum W_{pl,c} > 1.3\sum W_{pl,b} \quad (9)$$

Where $W_{pl,c}$ and $W_{pl,b}$ denote the plastic bending modulus of the columns and beams, respectively. Expression (8) is used for the middle joints while expression (9) is used for the peripheral joints. Results for criterion: "Strong columns/weak beams".

Table 1. Results for criterion: “Strong columns/weak beams”

k	$W_{pl,HEA340}$ =[1826cm^3]
$W_{pl,IPE400}$	$W_{pl,HEA340}/W_{pl,IPE400}$= 1.42>1.3
k	$W_{pl,HEA280}$ =[1088cm^3]
$W_{pl,IPE400}$	$2W_{pl,HEA280}/W_{pl,IPE400}$= 1.68>1.3

3.2 SECOND ORDER EFFECTS- (ULS)

In the following table (Table 2) are shown the values for the θ coefficient. According to the calculated values for the coefficient θ, it is noted that in storey 2, the value of $\theta = 0.13 > 0.1$. In other levels, the θ-coefficient for this example has values less than 0.1. Based on the current Eurocode 8, second-order effects are taken into account by amplifying the seismic actions.

Table 2. Values for θ coefficient according to linear static analysis

Story	$d_r = qd_e$	θ
1	37.2	0.09
2	55.2	**0.13**
3	49.7	0.10
4	37.8	0.07
5	20.8	0.037

3.3 CODE REQUIREMENTS FOR COLUMNS AND BEAMS

Depending on the cross-sectional class limitations, which is correlated with the q-factor, in order to avoid exceeding the plastic load-bearing and rotation capacity in a location where plastic hinges are expected to form, as a result of the mutual action of moments, the transverse and axial forces, Eurocode 8 also proposes some limits [3].

For a seismic combination, the applied moments, transverse forces, and axial forces in the beams are determined according to Equations in [3], where, to account for the second-order effects, $M_{Ed,E}$, $V_{Ed,E}$ and $N_{Ed,E}$ are amplified by 1/(1-θ). To achieve the "Strong Columns/Weak Beams" criterion, the calculated internal forces in the columns, from the elastic model, should be amplified by means of the coefficient Ω, which for Moment Frames (MRF) is given by the expression:

$$\Omega = \min\left(\frac{M_{pl,Rd,j}}{M_{Ed,j}}\right) \quad (10)$$

3.4 DAMAGE LIMITATION- SLS

The damage limitation criterion is checked for an earthquake with a probability of occurrence higher than the design earthquake. In this paper, in order to better understand the boundary behavior of the system, the limit of α = 1% is assumed, that is, the non-constructive elements are separated from the moment frame. The criterion is checked according to the equation [5]:

$$\alpha = \frac{d_e \cdot q \cdot v}{h} \quad (11)$$

Where, d_e, q and h are linear inter-storey drift, behavior factor and the inter-storey height, respectively. In the following, a tabular presentation of the relative floor displacements is given in accordance with the provisions of Eurocode 8. The factor v, which reflects the return periods of seismic actions, is assumed with a value of v = 0.5. Consequently, the structural damages from an earthquake from the SLS condition are "v" times smaller than the damage from an earthquake from the ULS condition.

Table 3. Damage limitation check for the analyzed frame

Level	$h[mm]$	$\frac{v \cdot q \cdot d_e}{h}(\%)$	Performace limit (%)
1	3000	0.62	$\alpha = 1$
2	3000	0.92	
3	3000	0.82	
4	3000	0.63	
5	3000	0.34	

According to the results shown, the closest to the damage limit are the relative storey displacements of level 2, which are 0.92<1 = α. Given that the θ coefficient in level 2 has the highest value ($\theta = 0.13$), such values were expected.

4. NON LINEAR STATIC ANALYSIS

In this paragraph, the example analyzed in point 3 is reanalyzed using non-linear static analysis. The non-linear static analysis was carried out with the software package SeismoStruct 2018. To simulate S235, the monoaxial model initially programmed by Yassin [1994] [10], which is based on the dependence proposed by Menegotto [7], [9], was used. The non-linear behavior of the steel is simulated with a reinforcement factor of 0.005.

The post-elastic behavior of beams and columns is simulated using the DP-Distributed plasticity formulation [4]. This is achieved by modeling the elements as non-elastic elements along their entire length and their non-linear properties are incorporated at the cross-sectional level. The global plastic behavior of the structure is obtained by integrating all cross-sections using shape functions built into the software package itself.

4.1 BEHAVIOUR OF GLOBAL SYSTEM

The global behavior of the system is represented by the Force-Displacement curve where a series of parameters are incorporated, such as: Lateral load at the appearance of the first plastic joint F_y, development and location of plastic joints and plasticization of the elements, Ultimate capacity F_u and the corresponding displacements at the occurrence of the first plastic hinge Δ_y and ultimate displacement Δ_u.

In Figure 2. Pushover curve for the considered construction is shown. The segment bounded by points O-A describes the linear-elastic behavior up to the limit of occurrence of the first plastic hinge (point A). The lateral load at the appearance of the first plastic hinge is F_y=381.72kN, while the corresponding displacement is Δ_y=118mm. The total design seismic load (including the effects of accidental torsion) from the linear elastic analysis is

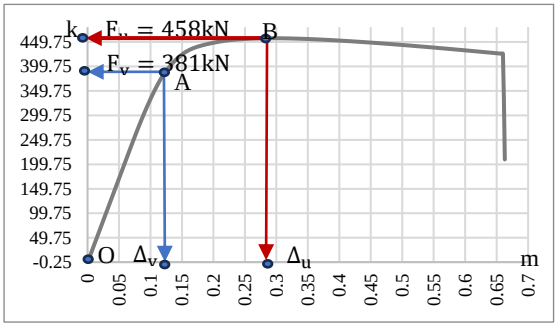

Figure 2. The Push-over curve for analysed steel moment frame.

S_{de}=188kN. Namely, for a seismic force almost 200% of the design action, the structure would remain in the linear elastic region.

The A-B portion of the curve is generated as a result of the plastic capacity to redistribute impacts until collapse is reached [6]. The ultimate state of the structure was reached from a total horizontal action of F_u=458kN and a corresponding displacement of Δ_y=291mm. The remaining part of the curve is called the softening branch and its gradient is functionally dependent on: The more sensitive the frame is to lateral loads, the steeper the drop will appear in the Push-Over Curve. In this case, a full mechanism is reached for a total displacement of 650mm.

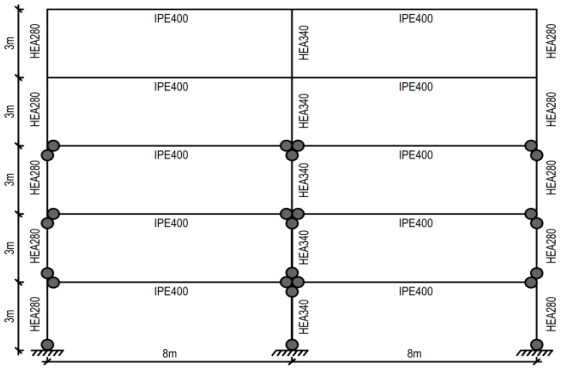

Figure 3. Distribution of plastic hinges over the MRF

Figure 3. shows the final stage of all plastic hinges in the construction while their development process is as follows: The first plastic hinge is registered in the first storey beam of the node with the peripheral column HEA280. The next plastic hinge is registered in the same vertical of the second storey. For columns, the first plastic joint is registered in the peripheral column HEA280 at the base of the structure. This is also a desirable way of initiating plasticization. Figure 3. shows the complete development of plastic joints and it can be easily noticed that in the last 2 levels of the frame, up to its ultimate state, no yielding of the elements was registered. This procedure leads to thinking about how to properly treat the "Strong columns/weak beams" criterion, which does not make a difference for the levels of the construction but must be fulfilled for each joint of the moment frame.

4.2 CALCULATION OF BEHAVIOUR FACTOR ACCORDING TO NONLINEAR STATIC ANALYSIS RESLUTLS

Based on the parameters extracted from Figure 2, the behavior factor for this construction is determined according to the Table 4. There is

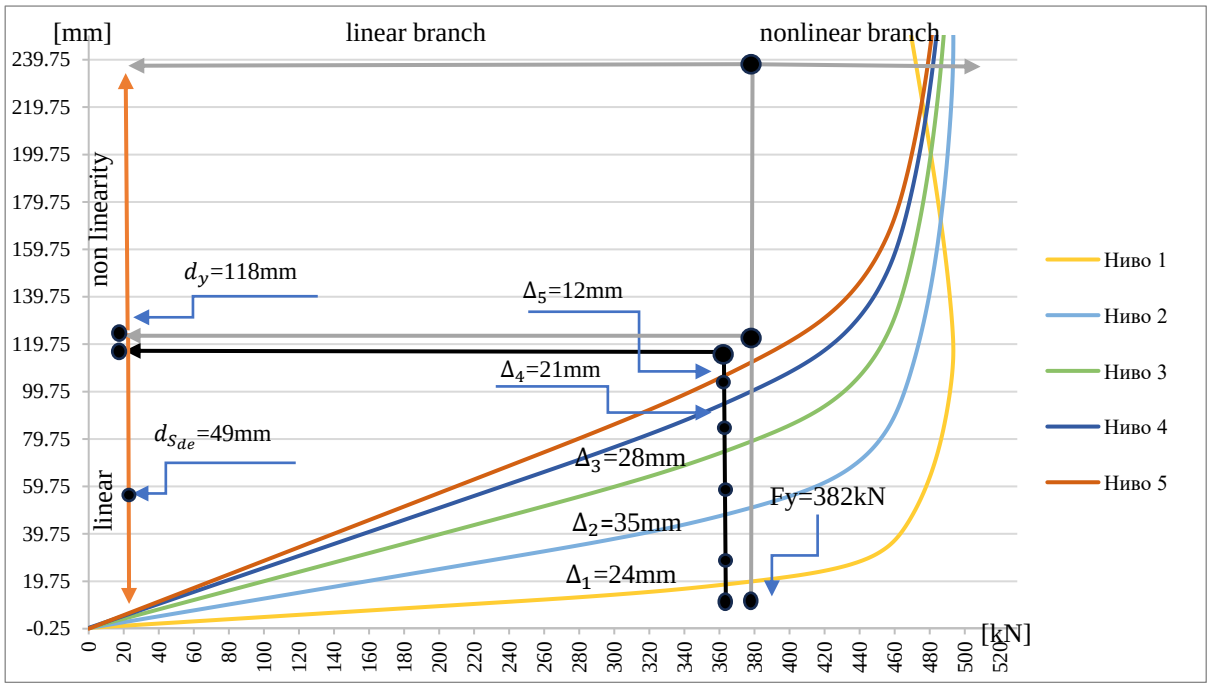

Figure 4. Distribution of lateral displacement of analyzed steel frame.

quite a large increase in the calculated value of the q-factor with the assumed value of q = 4. This is due to the solid ductility capacity of the system, which for structures with the period T > T_c is calculated according to the expression: $\mu = \frac{\Delta_u}{\Delta_y} = 2.46$, as well as due to the over strength factor, α = 1.2.

Table 4. Values for θ coefficient according to linear static analysis

F_b [kN]	F_y [kN]	F_u [kN]	$\alpha = F_u/F_y$	Δ_y [mm]	Δ_u [mm]	**q**
188	381.72	458	1.202	118	291	**6.5**

4.3 ANALYSIS OF LATERAL DISPLACEMENTS BY NONLINEAR STATIC ANALYSIS

Figure 4 shows the horizontal displacements of each storey under the influence of a lateral horizontal load. It is observed that the maximum relative storey displacements are registered for storey 2. As the frame levels progress, the curves are closer together. In level 2, a relative storey displacement of 35mm is observed and at that moment, the structure is already in a linear phase. In the case of moment frames, this criterion, in a large number of cases, is crucial for the selection of the cross-sections of the columns, so its interpretation has a key implication of the economy of the constructive solution. The existing Yugoslavian standards [8] for limiting horizontal displacements of the structural system, i.e H/500 (H-total height of the structure), for this example would dictate maximum displacements of 30 mm. On the other hand, the structure up to displacements of 118 mm is completely in the linear elastic region, although there are no special restrictions due to non-structural elements, such an approach would lead to an uneconomical solution.

5. CONCLUCSION

Using the principles of non-linear static analysis, an analysis of a Steel Moment Frame was performed which was pre-solved according to the provisions proposed by the current generation of Eurocode 3 and 8.

From the performed analyses, the following conclusions were drawn: The coefficient for sensitivity to floor displacements, calculated according to the current Eurocode 8 for level 2, requires the inclusion of second-order effects through the amplification of internal forces. On the other hand, according to the non-linear static analysis, the global behavior of the system is linear even for horizontal force up to F=380kN (2.02 times the design seismic force S_{de}=188kN). If the current formulation for the θ-coefficient is used, for level 3 , the inter-story displacements of 12.5mm imply a θ-coefficient with a value of 0.1 (Table 2). This is at the limit of including second-order effects. On the other hand, in level 3, for a load of 305kN, the

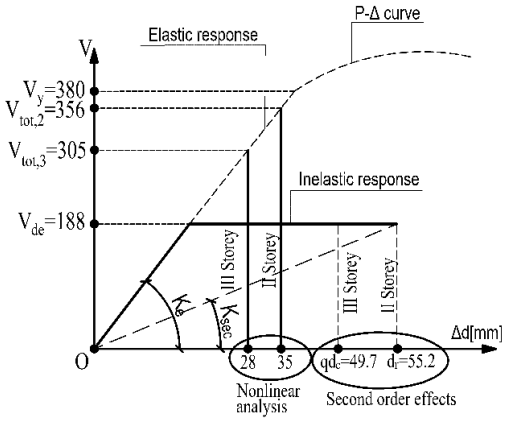

Figure 5. Display of horizontal displacements according to bilinear diagram (EC8) and non-linear static analysis.

considered structure (according to non-linear static analysis) behaves linearly (Figure 4 and Figure 5). This means that the relative storey displacements of 12.5(305/155.3) = 24.59 mm would belong to the area of linear elastic behavior. According to the conducted Pushover analysis, relative storey displacements up to 35mm imply elastic behavior of the structure in ULS condition. But according to current regulations, for displacements greater than 24.59 mm, it is necessary to take into account second-order effects through appropriate amplification (Table 2). Figure 5 shows how with this definition of secant stiffness according to EC8, displacements are obtained that lead to larger values for the θ-coefficient due to large values of inelastic displacements ($d_r = d_{eq}$).In the new generation of Eurocode 8, in the expression for θ, V_{tot} is amplified by the coefficient $k = q_S q_R$ which practically leads V_{tot} to the level of Significant Damage. For this example, significant damage can be considered the load close to the occurrence of first plastic hinge of the second storey beams. Given that the ratio Vy/S_{de} = 380/188 = 2.06, it follows that the initial values obtained for the θ-coefficient should be reduced by a value close to 2.

REFERENCES

[1] Denavit. M et al.: ,,Seismic performance factors for moment frames with steel- concrete compoiste columns and steel beam“. Earthquake engineering&structural dynamics. Wiley Online Library. DOI: 10.1002/eqe.2737.

[2] Eurocode 8: Design of Structures for Earthquake Resistance- Part 1: General rules, and rules for buildings.

[3] Eurocode 3: Design of steel structures - Part 1-1: General rules and rules for buildings.

[4] Gharakhanloo. A: “Distributed and concentrated inelasticity beam-column elements used in earthquake engineering”. Master Thesis, Civil and Environmental Engineering, NTNU-Tronheim, June 2014.

[5] Landolfo. R et al. :,,Design of steel structures for building in seismic areas”. Eurocode 8- Design of structures for earthquake resistance. Part 1-1- general rules, seismic actions and rules for buildings. ECCS. Wiley, 2016.

[6] Mazzolani. F, Piluso. V: ,,Theory and design of seismic resistanat steel frames”. Spon Press. Tylor & Francis Group, 1997.

[7] Menegotto M. et al (1973). „Method for analysis for cyclically loaded RC plane frames including changes in geometry and nonelastic behaviour of elements under combined normal forces and bending moments“. 15-22. Zurich, Switzerland.

[8] Pravilnik o Tehnickim Normativa Za Izgradnju Objekta Visokogradnje u Seizmickim Podrucijma, „Sluzbeni list SFRJ“. Br31/81, 49.82, 29/83,21/88 I 52/90.

[9] Yahmi. D, Branci. T, Bouchair. A and Fournely. E: “Evaluating the Behaviour Factor of Medium Ductile SMRF Structures”. Periodica Polytechnica, Civil Engineering. 62(2), pp. 375-385,2018.

[10] Yassin, M. H. M. (1994). “Nonlinear analysis of prestressed concrete structures under monotonic and cyclic loads.

Artur Roshi
PhD
Metropolitan University of Tirana
Albania
artur.roshi@yahoo.com

Golubka Nechevska - Cvetanovska
PhD, Emeritus Professor
Ss. Cyril and Methodius University in Skopje
Institute for Earthquake Engineering and Engineering Seismology
N. Macedonia

Jordan Bojadjiev
PhD, Assistant Professor
International Balkan University, Skopje
N. Macedonia

LABORATORY STUDY OF CONCRETE CYLINDERS CONFINED WITH CFRP

The field of research in the frames of this paper will be Application of Innovative Materials for Repair and Strengthening of RC Buildings in seismic active regions. Within the frames of this paper, special emphasis will be put on RC buildings where, during construction, the built-in concrete has not achieved the designed concrete class. In these cases, it is necessary to take measures for repair and strengthening of both individual structural elements and whole structures using traditional and Innovative Materials.

To present the possibilities and the benefits of use of these innovative construction materials in strengthening of structural elements of buildings and integral building structures, ample laboratory research for definition of the characteristics of these materials with different technologies of strengthening by CFRP (Carbon Fiber Reinforced Polymers) materials are carried out at the Institute of earthquake Engineering and Engineering Seismology – IZIIS, Skopje and Institute of Material Testing-ZIM-AD Skopje.

In this paper, technology of strengthening of RC columns with traditional materials as well as characteristics and types of innovative materials are introduced. Results from laboratory research of RC concrete specimens-cylinders with different technologies of strengthening by CFRP are presented.

Keywords: repair and strengthening, seismically active regions, traditional and innovative materials, concrete jacketing, compressive strength, elasticity module, CFRP

1. INTRODUCTION

Seismic strengthening of reinforced concrete structural elements represents one of the methods to increase the earthquake resistance of damaged or undamaged buildings. The strength of the structures can be moderately or significantly increased and the ductility can be improved, or in other words, it can be said that the concept of strengthening involves: a) increase in strength; b) increase in strength and ductility; and c) increase in ductility.

It has been a usual practice to perform repair, strengthening and rehabilitation of existing RC

buildings structures by application of traditional methods (most frequently, jacketing of elements), but lately, new innovative materials with a special technology of construction and repair have increasingly been applied. The application of these materials is still the subject of a large number of investigations worldwide, particularly in the field of application of these materials in seismically active regions.

In order to make a contribution towards development and application of new innovative materials in engineering practice, experimental, quasi-static tests were carried out in the Dynamic Testing Laboratory at UKIM-IZIIS – Skopje, R. Macedonia, and laboratory tests on materials were done at the Institute for Material Testing – ZIM, AD Skopje, R. Macedonia .

In this paper, at first traditional methods for strengthening of RC columns with jacketing, followed by detailed explanation of characteristics and types of innovative materials for strengthening of RC columns. At last, results are given from laboratory research and experimental investigations of RC concrete specimens-cylinders strengthened by CFRP with different technologies of strengthening by CFRP (Carbon Fiber Reinforced Polymers) materials.

2. REPAIR AND STRENGTHENING OF BUILDINGS USING TRADITIONAL MATERIALS

R/C jackets are applied in the case of serious damage or inadequate seismic resistance of the column (including here failure of quality of concrete used on the site during construction). Depending on the existing local conditions, jackets are applied along the perimeter of the column, which is the ideal case, or sometimes on one or more sides.

In case where the jacket is limited to the storey height, an increase in the axial and shear strength of the column is achieved with no increase in flexural capacity at the joints. Therefore, it is recommended that the jackets protrude through the ceiling and the floor slabs of the storey where column strengthening is necessary (Figure 1) [2].

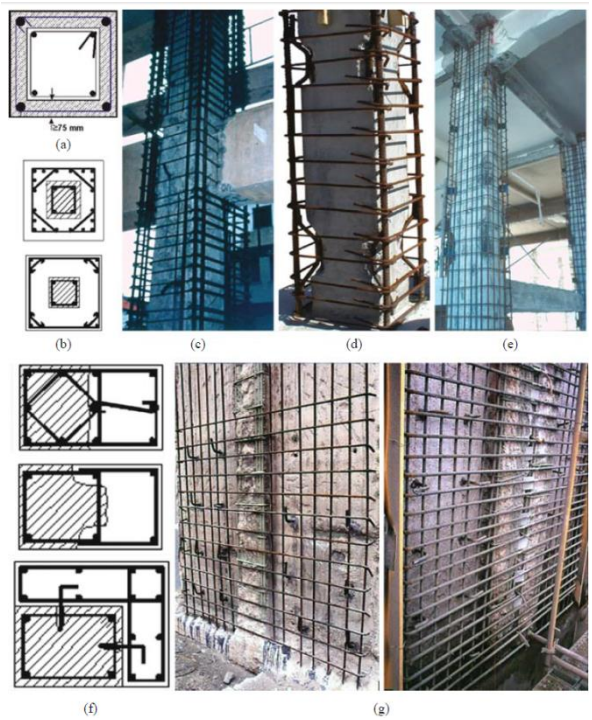

Figure 1. Concrete jackets in columns: a) simplest case b) jacket bars bundled near corners, engaged by cross-ties or orthogonal tie c) jacket bars bundled at corners, dowels at interface with old column d) U-bars welded to corner bars e) steel plates welded to corner bars f) one-or two-sided jackets g) one-sided concrete overlay with single curtain of two way reinforcement at exterior face of perimeter walls [2]

3. REPAIR AND STRENGTHENING OF BUILDINGS USING INNOVATIVE MATERIALS

3.1 FIBER REINFORCED POLYMERS (FRP)

FRP composites comprise fibers of high tensile strength within a polymer matrix. The fibers are generally carbon or glass, in a matrix such as vinylester or epoxy. These materials are manufactured to form plates under factory conditions, generally by a pultrusion process.

Reinforcement fibers are qualified in three main families of glass, aramid and carbon. There are other fibers, but they are relatively insignificant. The most important property of the fibers is their elastic modulus, and the fibres must be significantly stiffer than the matrix which allows them to carry most of the stress. Consequently, they must also be of high strength. Reinforcements are available in a variety of configurations of which there are three main categories:

- unidirectional, in which all the fibers lie in one direction.
- bidirectional, in which the fibres lie at 90° to one another. This is achieved either by use of woven fabric, non-woven fabric or by use of separate layers of fibres each unidirectionally, but successively laid at 90°.
- random, in which the fibers are randomly distributed and are in-plane.

Stress-strain fiber behaviour is different for every type of fiber (Figure 2) and different FRP shapes (Figure 3).

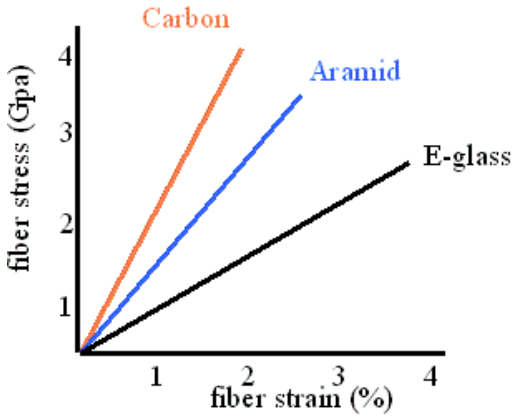

Figure 2. Stress- strain fiber behaviour [12]

3.2 CONFINEMENT STRENGTHENING

Confinement strengthening (Figure 4) consists of:

(1) Cleaning and repair
(2) Primer
(3) Adhesive
(4) FRP strips
(5) Last adhesive layer

Fiber polymer fabrics that can be used to improve bending, shear and axial capacities of the columns and beams may be manufactured from various materials such as carbon, glass and aramid without an increase in the volume of the strengthened member, significant improvements can be achieved in the capacity and ductility characteristics of the element.

These materials may practically be used for numerous purposes such as enhancement of the flexural capacity of floor slabs and improvement of shear capacity of beams, columns, joints and shear walls.

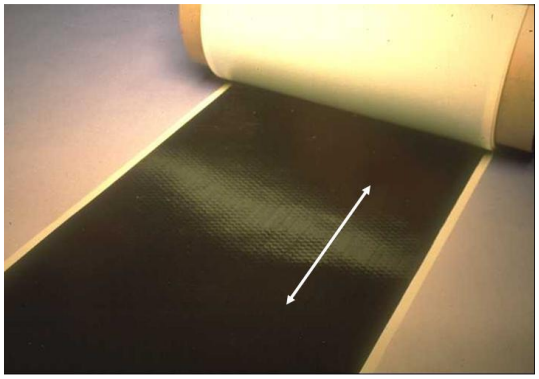

a)

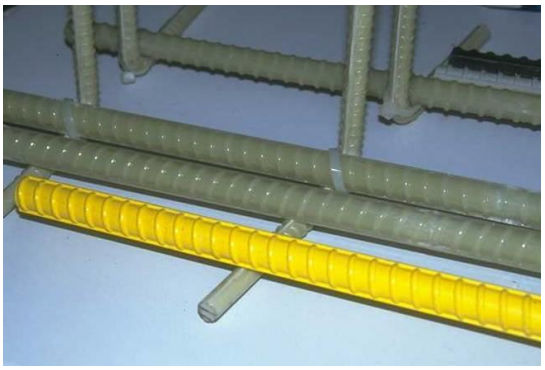

b)

Figure 3. Different FRP shapes a) sheet b) bars [12]

Figure 4. Confinement strengthening [5]

4. LABORATORY TESTS ON MATERIALS BUILT-IN MODELS FOR EXPERIMENTAL RESEARCH CARRIED OUT AT UKIM-IZIIS

To realize the experimental quasi-static tests, two models were designed and constructed, namely Model M1 and Model M2. The models were with identical proportions (supporting beam proportioned 50/50/116 cm and a column proportioned 30/30/200 cm), constructed to the scale of 1:1[13].

For the purpose of easier incorporation of the CFRP materials, it was decided to build the models in vertical position [3].

During concreting of the models, three trial specimens- concrete cubes proportioned 15/15/15 were taken from the supports - beams and three trial cubes proportioned 15/15/15 were taken from the columns, in addition to the nine (9) cylinders proportioned 15/30 cm (Figure 5). To define compressive strength and concrete class, laboratory tests were performed at stock holding company-GIM-Skopje (for the cubes) and ZIM –Skopje (for the cylinders), while the tests for definition of the modulus of elasticity of the built-in concrete were done at ZIM – Skopje, Macedonia [13].

Figure 5. Photos of taken trial concrete specimens (cylinders)

Using the trial concrete specimens – cylinders, three series of tests of compressive strength and tests for definition of the modulus of elasticity of the built-in concrete were carried out as follows:

- Series 0- concrete cylinders without CFRP- plain concrete
- Series 1- concrete cylinders wrapped with 1 (one) CFRP layer
- Series 2- concrete cylinders wrapped with 2 (two) CFRP layers

Presented further are photos and results taken during laboratory tests for definition of compressive strength of concrete for the three series (Figure 6 and Figure 7). It must be pointed out that the collapse of the models from the first and the second series was explosive, with big crushing of concrete wrapped with CFRP. This was particularly pronounced in Series 2 where concrete was wrapped with two CFRP layers.

4.1 RESULTS FROM TESTS FOR OBTAINING THE COMPRESSIVE STRENGTH OF CONCRETE CYLINDERS

Parallel with the performed tests on the three series, the obtained results on failure forces and the results from computation of compressive strength of all three series of concrete cylinders were recorded in special tables (Table 1).

Figure 6. Preparation of strain gauges on concrete cylinders.

From the results obtained, it can be concluded that the force inducing failure of concrete

cylinders without CFRP amounts to 296.0 kN. For the cylinder with one CFRP layer, it amounts to 670.0 kN., while for the cylinder with two CFRP layers, it amounts to 955.0 kN. The compressive strength amounts to 16.8 MPa, 37.0 MPa and 54.1 MPa, for all three series, respectively.

Figure 7. Testing of compressive strength of concrete wrapped with two CFRP layers- the 2nd series.

Table 1. Compressive strength of three series of concrete cylinders.

Date of casting: 04.10.2019 Date of testing: 15.11.2019 Concrete cylinders CC (3 series) 15/30 cm					
Series		**Proportions H/D [cm]**	**Weight (g)**	Failure force [kN]	**Compressive strength [MPa]**
Specimens	**0**	30/15	12200	296.0	16.8
	1	30/15	12700	670.0	37.9
	2	30/15	12800	955.0	54.1

In general, it can be concluded that the compressive strength is higher with the number of CFRP layers.

4.2. RESULTS FROM TESTS FOR OBTAINING THE ELASTICITY MODULUS

Testing of the static modulus of elasticity for each series (0, 1, 2) of built-in concrete was also done in the laboratory of the Institute for Testing Materials – ZIM – Skopje AD. The tests for obtaining the static modulus of elasticity under pressure were performed according to MKS U.M1.025. The most relevant for estimation of the static modulus of elasticity was the mean value of the recorded entries of the strain gages, after dissolution in the last cycle.

Presented further are some of the photos taken during the tests on the three series of concrete cylinders (Figure 8).

Figure 8. Testing of the static modulus of elasticity of all three series.

Generally, it can be concluded that the obtained values for the concrete cylinders with one and two CFRP layers are higher than the values obtained for the concrete cylinders without CFRP.

5. CONCLUSIONS

In the paper part of the analytical, laboratory and experimental investigations of designed

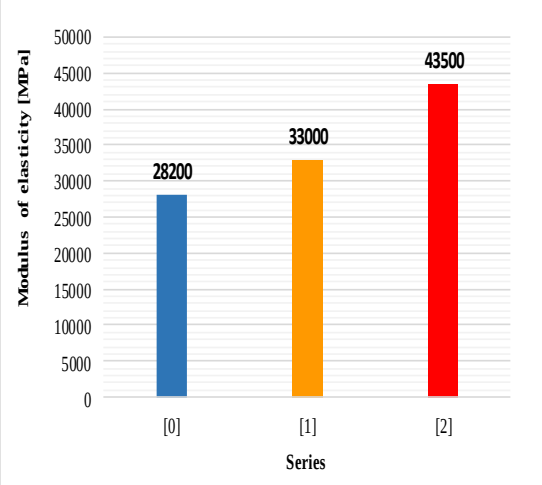

Figure 9. Testing of the static modulus of elasticity of all three series.

models of RC columns strengthened with CFRP were presented. Based on the experimental investigations the following conclusions can be outlined:

- The force inducing failure of concrete cylinders without FRP amounts to 29.6 t, i.e., 296 KN. For the cylinder with one FRP layer, it amounts to 67.0 t, i.e., 670 KN, while for the cylinder with two FRP layers; it amounts to 95.5, i.e., 955 KN. The compressive strength amounts to 16.8 MPa, 37.0 MPa and 54.1 MPa, for all three series, respectively.
- In general it can be concluded that the compressive strength and Module of elasticity is higher with the number of FRP layers.
- Obtained values for the concrete cylinders with one and two CFRP layers are higher than the values obtained for the concrete cylinders without CFRP.
- These tests are good basis for further analytical and numerical investigations that can provide additional conclusions.

REFERENCES

[1] CNR-DT 200/2004. Guide for the Design and Construction of Externally Bonded FRP Systems for Strengthening, 2004 (Downloaded free from:http://www.cnr.it/sitocnr/IICNR/Attivita/NormazioneeCertificazione/NormazioneeCertificazione file/IstruzioniCNR DT200 2004 eng.pdf).

[2] Fardis, M. N., Biskinis, D., Kosmopoulos, A., Bousias, S. N., & Spathis, A. S. (2005). Seismic retrofitting techniques for concrete buildings. In Proceedings of SPEAR Workshop–An event to honour the memory of Jean Donea (MN Fardis and P. Negro, eds.) (pp. 229-240).

[3] Krstevska, L., Nechevska- Cvetanovska, G. (2019), Quasi-static testing of column models strengthened by FRP, UKIM-IZIIS, IZIIS Report 2019-75.

[4] M. DI ludovico, A. Prora, G.Manfredi and E.Gosenza, “Seismic Strengthening of an Under-design RC Structure with FRP”, Department of Structural Engineering, University of Naples Federico II, Naples, Italy, Published online 24 August 2007 in Wiley InterScience.

[5] Di Ludovico M. *“Design and Retrofit of RC Constructions”,* lecture notes, Department of Structural Engineering, University of Naples Federico II, 2013.

[6] G. Necevska-Cvetanovska and R. Petrushevska (2000). “ Methodology for Seismic Design of R/C Building Structures “. 12WCEE, New Zeland.

[7] Necevska-Cvetanovska, G., Apostolska, R. (2012). Methodology for Seismic Assessment and Retrofitting of RC Building Structures, Proc. of 15 World Conference on Earthquake Engineering (Paper ID 2149), 24-28 September 2012, Lisboa, Portugal.

[8] Nechevska-Cvetanovska, G., & Roshi, A. (2019). Rehabilitation of RC buildings in seismically active regions using traditional and innovative materials. Građevinski materijali i konstrukcije, 62(3), 19-30.

[9] Nechevska-Cvetanovska, G., Roshi, A., & Bojadjieva, J. (2019). Seismic strengthening of existing rc buildings structures using concrete jacketing and frp materials. E-GFOS, 10(19), 68-80.

[10] Necevska – Cvetanovska, G., Roshi, A. “Rehabilitation of RC Buildings in seismically Active Regions Using Traditional and Innovative Materials”, Journal Building Materials and Structures, Novi Sad, Serbia, 62 (2019) 3 (19-30).

[11] Roshi, A., Nechevska- Cvetanovska, G. (2019). Repair and Strengthening of RC Buildings using Traditional and Innovative Materials, 18th International Symposium organized by Macedonian Association of Structural Engineers (MASE), October 4-7, 2019, Ohrid, Macedonia.

[12] Andrea Prota “*Innovative Building Materials*”, lecture notes, Department of Structural Engineering, University Federico II, Naples, 2014.

[13] Roshi, A., (2020). Application of innovative buildings materials for repair and strengthening of rc columns in seismically active regions, Doctoral dissertations, Ukim Iziis Skopje, Macedonia.

Todorka Samardzioska
PhD, Full Professor
Ss. Cyril and Methodius University in Skopje
Faculty of Civil Engineering
N. Macedonia
samardzioska@gf.ukim.edu.mk

Andrea Velkova
MSc in Civil Engineering
Civil Engineering Institute Macedonia - Skopje
N. Macedonia

Ivan Naumovski
MSc in Civil Engineering
Civil Engineering Institute Macedonia - Skopje
N. Macedonia

Milica Jovanoska - Mitrevska
PhD, Assistant Professor
Ss. Cyril and Methodius University in Skopje
Faculty of Civil Engineering
N. Macedonia

Nikola Postolov
MSc, Teaching Assistant
Ss. Cyril and Methodius University in Skopje
Faculty of Civil Engineering
N. Macedonia

Riste Volchev
MSc, Teaching Assistant
Ss. Cyril and Methodius University in Skopje
Faculty of Civil Engineering
N. Macedonia

THERMAL PROPERTIES OF SUSTAINABLE CEMENT COMPOSITES WITH STRAW

Energy efficiency, energy saving, recycling and reuse of materials and reducing the harmful impact of buildings on the environment, influence the idea of implementing composites that include ecological matrixes in daily construction operations, using natural or recycled materials. Straw is a widely available by-product of agricultural activity. By recognizing the properties of the straw, as well as other agro-waste materials, a new dimension is given to the thermal insulation of buildings. Furthermore, the building becomes highly efficient, sustainable and with lower costs.

Standardized samples of cement composites were tested and analysed, with partial replacement of the first fraction of the aggregate with straw in the range of 5%, 10%, 20% and 50%, with emphasis on the thermal properties. Thermal conductivity decreases with an increase in the percentage of straw in the cement composite. The average value for thermal conductivity for all samples is 0.310 W/m·K. The recipe with a share of 20% straw as a substitute for the smallest aggregate, proved to be the most suitable recipe, which also showed good mechanical properties. Its thermal conductivity is λ = 0.223 W/m·K, that is about 10 times lower than the thermal conductivity of ordinary concrete. However, with an increase in the percentage of straw, the compressive strength decreases. Therefore, the application of this type of material is limited to non-bearing structural elements.

Keywords: thermal conductivity, agro concrete, straw, sustainability

1. INTRODUCTION

The research activity nowadays is significantly directed towards the study of lightweight composites using plant materials instead of cement or aggregate. In this way, building materials and construction products are obtained that are characterized by lower density and lower thermal conductivity. Natural organic products have great potential to mitigate the carbon footprint left by conventional materials such as concrete, steel, polymers and ceramics during their production

and processing, recognizing straw as one of the most significant substitutes, due to its wide availability as a by-product of the large agricultural activity at the local and global level. It has been proven in many studies that thermal insulation materials based on natural fibres have competitive thermal properties, such as heat capacity or thermal conductivity, compared to traditional thermal insulation materials.

One of the characteristics of sustainable and green buildings is the application of strategies based on technologies that favour the conservation of water, energy, and materials. These strategies include the use of energy-efficient equipment, alternative energy sources and low-energy materials. The second approach refers to the development of building materials from agro-waste. Using agro-waste to develop building materials reduces the pollution generated in the construction industry and helps to deal with waste disposal, which burdens the agricultural industry.

The aggregate is about 60-80% of the volume of the concrete; therefore, such enormous requirements attract attention and preservation of the natural aggregates, which are subject of serious concern. Straw, sugarcane bagasse ash, rice husk, cane, sawdust, peanut shell, oyster shell, tobacco waste, palm oil ash, coconut shell, etc. are part of the agricultural waste (or bio-waste in general) that can be used as a partial or full replacement of the aggregate in the concrete mix, and has been processed in many scientific studies. Studies by Chennakesava Rao & Prabath [1], Rahim et al. [2], Petkova-Slipets et al. [3], Shea et al. [4] are some of them.

2. MATERIALS AND METHODS

1.1 SUSTAINABLE STRAW

Straw is one of the oldest and most used materials for construction, the application of which remains current even today. This is a result of its wide availability, cost-effectiveness, sustainability and low carbon footprint. Straw is a material with low density and low thermal conductivity, thanks to its porous internal structure.

Usually, natural materials, classified as agro-waste, have a lower value of the thermal conductivity λ, unlike traditional materials.

The direction of stretching of the straw fibers in relation to the heat flow, in certain construction applications, such as straw bales, also has a great influence on the value of the thermal conductivity. The German national organization for building with straw bales FASBA [5], based on a series of researches, presents a value of λ = 0.080 W/m·K when the fibres are placed parallel to the heat flow and λ = 0.043 W/m·K when the fibres are placed perpendicularly, Fig. 1. When the fibres are placed normally, the heat flow trajectory increases, i.e. the thermal conductivity decreases.

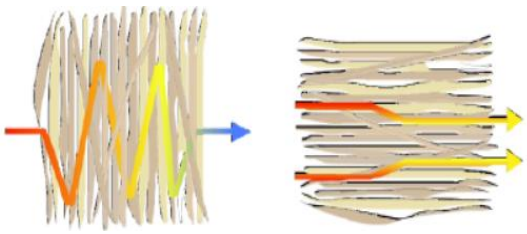

Figure 1. Heat flow in relation to the straw fibres orientation: a) perpendicular, b) parallel (FASBA [5])

1.2 SAMPLE PREPARATION

Testing the thermal properties of the cement composite with straw admixture implied preparation of 3 samples for each of the formulations, in which volume replacement was performed at 5%, 10%, 20% and 50% respectively of the volume of the aggregate (fraction 0-4 mm) with straw. Thermal properties were investigated on samples with dimensions at its base of 300 mm x 300 mm. They were kept in the laboratory for 28 days under standard conditions, until the composite hardens completely [6]. The main goal is to investigate the influence of the different percentage of straw on the thermal properties of this type of composite.

All materials used in the experimental research are in accordance with the current standard for concrete production and definition of concrete as a construction product MKS EN 206. Cement type CEM I 52.5 R was used as a binder. It is pure Portland cement with a small addition of gypsum to regulate setting time and up to 5% other mineral additives. It is characterized by high strength characteristics (in the early and late stages), but also by a relatively high heat of hydration. The aggregate used is with a maximum grain diameter of 16 mm obtained in the production facility, Govrlevo limestone mine.

Natural rice straw is taken as waste from a processing plant. It was cut into small pieces of no specific length, stored in a dry state and in a room with low humidity, Fig. 2. In general, straw as a material contains large amounts of

cellulose, hemicellulose and lignin. This research was conducted with chemically untreated straw, even though many researchers recommend treating the straw with chemical solutions, in order to reduce the problems connected to hydration and hardening of the cement. The amount of water was defined during the mixing itself in order to obtain a homogeneous mixture.

Figure 2. Straw and preparation of samples

Figure 3. Fresh concrete samples for testing thermal conductivity

1.3 MEASUREMENT OF THERMAL CONDUCTIVITY

Testing of the thermal properties of the cement composites was performed in the Laboratory of the Faculty of Civil Engineering in Skopje. The Heat flow meter (HFM) instrument, Fig. 4, was used to measure the thermal conductivity λ of the samples that are subject of this research. Its temperature range ranges from -20 °C to +100 °C, and 0.5 W/m·K is the maximum thermal conductivity it can measure.

The heat flow measurement method is a standardized test technique. The following standards were used: MKS ISO 8301:2016 [7], MKS EN 12667:2009 [8] and MKS EN 12939:2009 [9].

Actually, the sample is placed between a hot and cold plate, then a temperature gradient is applied and the heat flow through the sample is measured, [10]. Already calibrated heat flux sensors measure the heat flux (q) of the test sample. Since the two plates of the instrument are set at different temperatures, the test ends after thermal equilibrium has been established in the sample, i.e., after heat transfer has ended.

Figure 4. Instrument HFM

The heat flux q (W/m^2) is the rate of heat transfer in the x direction per unit area and is proportional to the temperature gradient ($\Delta T/\Delta x$) in this direction. The proportionality constant is the heat transfer property of the material, known as thermal conductivity.

$$q = -\lambda \frac{\Delta T}{\Delta x} \quad (1)$$

3. RESULTS

The samples with 5% straw are with different densities of 1989, 1905 and 1950 kg/m^3, respectively, as shown in Table 1. To determine the thermal conductivity, two of these samples were examined, however, the examination did not converge to a constant value for both. Actually, they showed a thermal conductivity greater than 0.5 W/m·K, which is the upper limit of the measurement equipment.

Three samples were also made from the second mixture, for which volume replacement was performed from the first fraction of the aggregate (0-4 mm) with 10% straw. The measured thickness of the samples is 6.5 cm for the first sample and 5.5 cm for the other two. The density differs for all three samples: 1758 kg/m^3, 1583 kg/m^3 and 1758 kg/m^3, respectively. Figure 5 shows the comparison of the obtained results for the thermal conductivity (λ) for all three samples with a percentage of straw of 10% and their mean value was calculated.

The obtained value of the thermal conductivity does not have a large variation among the three samples with 10 % straw. The calculated mean value for $\lambda_{10\%}$ is 0.441 W/m·K.

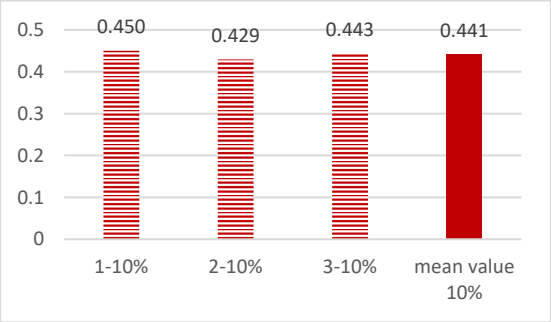

Figure 5. λ for samples with 10% straw

The measured densities for the series of examined samples with 20% of straw are 1288 kg/m^3, 1322 kg/m^3 and 1419 kg/m^3, respectively. The thicknesses of the samples are 5.2 cm, 5.4 cm and 4.5 cm. Figure 6 shows the results obtained for the samples where the aggregate was replaced with 20% straw.

The calculated mean value for the thermal conductivity is $\lambda_{20\%}$ = 0.223 W/m·K. The average temperature during examination of the samples is 20.53 °C, and the average value of the temperature difference between the two plates of the instrument is 19.56 °C. The average value for the thermal resistance *R* for the three samples is 0.2407 m^2/W·K.

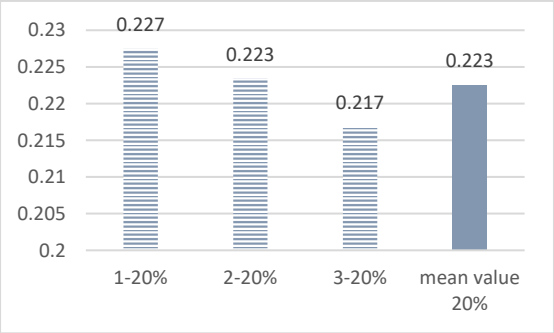

Figure 6. λ for samples with 20% straw

For testing the thermal characteristics in which straw replaces half of the aggregate volume or 50%, three samples were also prepared, but two of them experienced failure due to their own weight as a result of the inhomogeneity of the prepared mixture. The thermal conductivity, however, was investigated on the remained one sample (Figure 7), in order to make a comparison with the other samples in terms of how the percentage of straw affects the cement composites. The thickness of this sample is 6 cm, and the calculated density compared to other samples is the smallest: 1142 kg/m^3.

Figure 7. Sample with 50% straw

The test results are shown in Figure 8. The obtained thermal conductivity is λ = 0.1833 W/m·K, while the thermal resistance *R* is 0.567 m^{2}K/W.

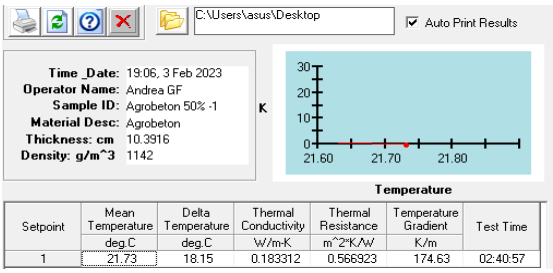

Figure 8. Results for the sample with 50% straw

4. ANALYSIS OF THE RESULTS

The obtained results for the thermal conductivity for all tested samples are shown in summary in Table 1 and in Figure 9.

Table 1. Density and thermal conductivity for all samples

sample	participation of straw [%]	density [kg/m^3]	thermal conductivity [W/m·K]
5% - 1	5%	1989	> 0.5
5% - 2	5%	1905	> 0.5
5% - 3	5%	1950	> 0.5
10% - 1	10%	1602	0.450085
10% - 2	10%	1583	0.429384
10% - 3	10%	1758	0.442659
20% - 1	20%	1288	0.227459
20% - 2	20%	1322	0.223422
20% - 3	20%	1419	0.216817
50% - 1	50%	1142	0.183314

In the research carried out and the results shown, the different percentage participation of straw in the creation of the cement composite affects the value of its thermal conductivity. The obtained results show that the lowest value of λ occurs in the tested sample with 50% straw, and the highest value occurs in sample 1 in which replacement is made with 10% straw. Increasing the percentage of straw decreases the thermal conductivity. Namely, the calculated mean value for λ for the samples with a share of only 10% straw as a substitute for the smallest aggregate is 0.441 W/m·K. The calculated mean value for the thermal conductivity for the samples with 20% straw, on the other hand, is λ = 0.223 W/m·K. The double share of straw gives almost twice lower thermal conductivity for the cement composite. This is due to the excellent thermal characteristics of straw.

The participation of 50% straw as a substitute for aggregate in the first fraction led to a decrease in the thermal conductivity to a value of 0.183 W/m·K. However, from the point of view of load-bearing capacity and durability, the sample with 50% straw does not show any strength characteristics, so its further application should be limited or subjected to further tests.

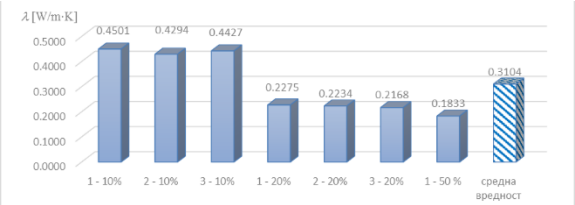

Figure 9. Thermal conductivity for all tested samples

Figure 9 also shows that for the samples in which the same percentage replacement of straw is carried out, the thermal conductivity values do not have a large variation. The mean value obtained from all seven samples is λ = 0.310 W/m·K.

The density of the material is one of the main factors affecting thermal conductivity. Increasing the percentage of straw decreases the density of the samples. The sample with 50% straw has the lowest measured density of 1142 kg/m^3. This is expected, knowing the porous structure of straw.

In this study, no directly proportional dependence between the thermal conductivity and density was established. Although it can be concluded that it is a very small difference in the densities, unlike the percentage of straw, it has no practical effect on the thermal conductivity, which may be due to the inhomogeneity of the material. However, Fig. 10 shows that the increase in density gives a general trend of increasing the thermal conductivity.

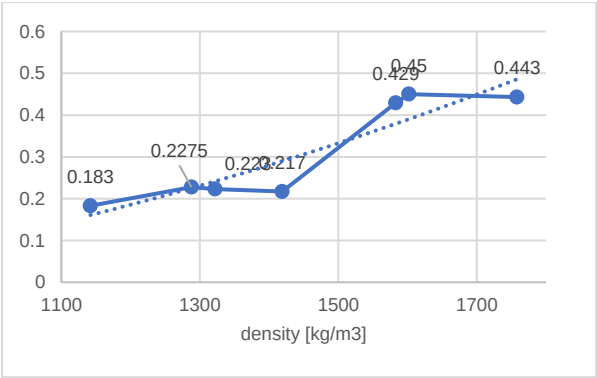

Figure 10. Thermal conductivity [W/mK] versus density

Finally, the cement composite that is subject of this research shows much lower thermal conductivity compared to traditional building materials. For comparison, concrete has a thermal conductivity of 2.0 – 2.5 W/m·K, and for reinforced concrete the value reaches up to 3.2 W/m·K. According to some research, increasing the percentage of reinforcement affects its value, because steel is characterized as a material with high thermal conductivity.

5. CONCLUSIONS

In this paper, the thermal properties of sustainable agro-concrete with the participation of straw, the most widely available agricultural by-product in our area, have been elaborated. Different mixtures of cement composite were tested in which the volume of the first fraction of the aggregate was partially replaced with 5%, 10%, 20% and 50% straw. The experimental test was performed according to a standardized procedure, with the instrument Heat Flow Meter.

From the obtained results, it can be concluded that the thermal properties of this composite are much better than traditional construction concrete. The thermal conductivity decreases with an increase in the percentage of straw in the cement composite. The average value for the thermal conductivity for all samples is 0.310 W/m·K. As the most appropriate recipe, which showed good mechanical properties also, the recipe with a participation of 20% straw as a substitute for the smallest aggregate is chosen. Its average thermal conductivity is λ = 0.223 W/m·K. The favourable heat-insulating

characteristics are mostly due to the porous structure of the straw.

On the other hand, as the percentage of straw increases, the strength decreases. Therefore, the recommendation is that this type of material should be limited to non-bearing structural elements. The application of this composite would be most acceptable in infill blocks in partition and facade walls, in order to make the most of its potential for good thermal insulation.

The general conclusion that can be drawn from the presented paper is that the cement composite with a percentage of straw shows excellent thermal properties and justifies the use of straw in buildings construction. This type of cement composite has competence and potential for application in everyday construction practice, and considering that straw is a widely available by-product at a low price, it can show high competitiveness in the market of insulation materials. At the same time, cement composites that incorporate renewable resources such as straw into their matrix will generate a positive footprint on the environment and help eradicate the negative impact that the construction industry has had so far.

Acknowledgements

The authors express their gratitude to the employees of the Laboratory in GI "Macedonia" for the overall material, spatial and personnel support during the preparation of the samples.

REFERENCES

[1] Chennakesava Rao M.S. & Prabath N.V.N. (2015). Green Concrete using Agro Industrial Waste (Sugarcane Bagasse ASH). Int. J. Soft Comput. Eng. (IJSCE), 5(1), pp. 86–92.

[2] Rahim N. L. et al. (2020). Investigation of bamboo as concrete reinforcement in the construction for low-cost housing industry. IOP Conf. Ser.: Earth Environ. Sci. 476 012058.

[3] Petkova-Slipets R. et al. (2020). A comparative thermal analysis of wallscomposed of traditional and alternative building materials. Civ. and Env. Eng. 16 (2), pp. 388-395.

[4] Shea A.D. et al. (2013). Evaluation of the thermal performance of an innovative prefabricated natural plant fibre building system. Building Services Engineering Research & Technology, 34 (4).

[5] FASBA. (2019). Straw Bale Building Guidelines, pp. 11-15. (available at www.fasba.de).

[6] Velkova A. (2023). Thermal properties of sustainable composit cement material with straw. MSc Thesis (supervisor: Samardzioska T.), Faculty of Civil Engineering, UKIM, Skopje.

[7] MKS ISO 8301:2016 Thermal insulation — Determination of steady-state thermal resistance and related properties — Heat flow meter apparatus.

[8] MKS EN 12667:2009 Thermal performance of building materials and products - Determination of thermal resistance by means of guarded hot plate and heat flow meter methods - Products of high and medium thermal resistance.

[9] MKS EN 12939:2009 Thermal performance of building materials and products - Determination of thermal resistance by means of guarded hot plate and heat flow meter methods - Thick products of high and medium thermal resistance.

[10] Samardzioska T., Jovanoska-Mitrevska M., Grujoska V. (2024): “Sustainable Mortars with Slag for Green Facades”, Current Trends in Civil & Structural Engineering. 10(4): 2024. CTCSE.MS.ID.000741. DOI: 10.33552/CTCSE.2024.10.000741.

SJCE

SCIENTIFIC JOURNAL OF CIVIL ENGINEERING

SS CYRIL AND METHODIUS UNIVERSITY
FACULTY OF CIVIL ENGINEERING